J. Fluid Mech. (2003), *vol.* 476, *pp.* 223–265.
DOI: 10.1017/S0022112002002926 Printed in the United Kingdom

Flow along streamwise corners revisited

By A. RIDHA

Laboratoire de Mécanique, Université de Caen, BP 5186–14032 Caen Cedex, France and
Laboratoire de Modélisation en Mécanique, CNRS: UMR 7607, Université Paris 6,
Tour 66 – Case 162, 4 place Jussieu, 75252 Paris Cedex 05, France
ridha@meca.unicaen.fr

(Received 29 June 1999 and in revised form 10 June 2002)

In this paper we investigate the three-dimensional laminar incompressible steady flow along a corner formed by joining two similar quarter-infinite unswept wedges along a side-edge. We show that a four-region construction of the potential flow arises naturally for this flow problem, the formulation being generally valid for a corner of an arbitrary angle $(\pi - 2\alpha)$, including the limiting cases of semi- and quarter-infinite flat-plate configurations. This construction leads to five distinct three-dimensional boundary-layer regions, whereby both the spanwise length and velocity scales of the blending intermediate layers are $O(\delta)$, with $Re^{-1/2} \ll \delta \ll 1$, Re being a reference Reynolds number supposed to be large. This reveals crucial differences between concave and convex corner flows. For the latter flow regime, the corner-layer motion is shown to be mainly controlled by the secondary flow which effectively reduces to that past sharp wedges with solutions being unique and existing only for favourable streamwise pressure gradients. In this regime, the corner-layer thickness is shown to be $O(Re^{-0.5+\alpha/\pi}/\delta^{2\alpha/\pi})$, $-\frac{1}{2}\pi \leqslant \alpha \leqslant 0$, which is much smaller than $O(Re^{-1/2})$ for concave corner flows.

Crucially, our numerical results show conclusively that, for $\alpha \neq 0$, closed streamwise symmetrically disposed vortices are generated inside the intermediate layers, confirming thus the prediction made by Moore (1956) for a rectangular corner, which has so far remained unconfirmed in the literature.

For almost planar corners, three-dimensional corner boundary-layer features are shown, as in (Smith 1975), to arise when $\alpha \sim O(1/\ln Re)$. On the other hand, we show that the flow past a quarter-infinite flat plate would be attained when both values of the streamwise pressure gradient and external corner angle $(\pi + 2\alpha)$ become $O(1/\ln Re)$ or smaller.

Numerical results for all these flow regimes are presented and discussed.

1. Introduction

Flow along streamwise (concave and convex) corners provides a realistic model to many engineering applications such as wing–body junctions, wind tunnel corners, box-like inlet configurations or sharp edges. Related previous works have, in general, been mainly focused on the zero pressure gradient laminar boundary-layer motion along concave corners formed by two intersecting semi-infinite planes with coplanar leading edges. This problem was first considered by Loitsianskii (1936), and then by Loitsianskii & Bolshakov 1936, who employed approximate integral methods. However, the first real attempt to satisfy boundary-layer equations was undertaken by Carrier (1947) who used only the streamwise momentum equation, and satisfied the

continuity equation through an assumption relating the three velocity components. This shortcoming was then overcome by Pearson (1957) by using the full three-dimensional boundary-layer equations, and deriving correct corner-layer boundary conditions in exploiting the asymptotic form of the vorticity equation. Yet, it was Rubin (1966) who produced the first fully rigorous analysis by employing the matched asymptotic expansions method to derive the far-field boundary conditions for the corner layer, followed by demonstrating the algebraic decay nature of the similarity equations (Pal & Rubin 1971), before eventually focusing on their numerical solution (Rubin & Grossman 1971). Other numerical solutions were also computed by Desai & Mangler (1974), Ghia (1975), Barclay & Ridha (1980), and by Wilkinson & Zamir (1984) amongst others. Desai & Mangler (1974) made the reasonable assumption that at large distances from the corner the boundary layer becomes precisely two-dimensional, but their application was unfortunately made in the boundary-layer sense, and by consequence defeated its purpose. Using their formulation, Ridha (1978) highlighted this shortcoming and gave a derivation for the correct far-field boundary conditions. This probably explains why their result is found to diverge considerably from those of other authors, particularly with regard to the secondary flow.

For the non-zero pressure gradient corner flow counterpart, it appears that the first rigorous work is due to Smith (1975) who examined the three-dimensional stagnation point flow into a corner of angle $(\pi - 2\alpha)$. He demonstrated that three-dimensional corner viscous flow features are produced when $\alpha \sim O(1/\ln Re)$, Re being a reference Reynolds number supposed to be large. Much later, Ridha (1990) considered a corner flow with external streamwise velocity component proportional to z^m (z being the streamwise distance measured from the leading edge and m an arbitrary constant), derived similarity solutions for the right-angle corner configuration, and presented numerical solutions valid at the corner-layer side-edge; these were found to be different from the classical Falkner–Skan family of solutions (Rosenhead 1966), non-unique, existing only for $\beta \geqslant -0.03678$, and including a three-dimensional solution besides the Blasius one (when $m = 0$), $\beta = 2m/(1 + m)$ being the Falkner–Skan parameter. Motivated by the (subsequent) question of the match between the Falkner–Skan solution and that prevailing at the corner-layer side-edge, Ridha (1995) investigated the corresponding potential flow problem, and demonstrated that a four-region construction was required for its analysis.

Dhanak & Duck (1997) have investigated the effects of free-stream pressure gradient on symmetrical as well as asymmetrical boundary layers in rectangular corners, and on their flow stability. They found that non-uniqueness was a common feature of the corner-layer similarity solutions; conditions at the corner-layer side-edge turned out to be essentially the same as those of Ridha (1990, 1992) for symmetrical corner flows.

On the experimental side, the works of El-Gamal (1977) and Zamir (1981) for the rectangular corner and Barclay (1973) for the 135° corner situations provide results against which a meaningful comparison with theoretical predictions can be made. This appears to be vindicated by the close resemblance between them and the lower solution branch results of Dhanak & Duck (1997) for the rectangular corner case.

Our objective in the present work is to consider the general combined potential and viscous flow problems along corners of arbitrary included angle $(2\pi > \pi - 2\alpha > 0)$ for non-zero streamwise pressure gradient, including the semi- and quarter-infinite flat-plate limits, and to address the question of transition from the Falkner–Skan solution, arising sufficiently far away from the corner, to that prevailing at the

corner-layer side-edge. We therefore begin by analysing the potential flow in § 2 where four-region treatment is shown to be required (see figure 1), revealing thus its singular perturbation type character. The boundary layer is then analysed in § 3, where a five-region treatment turns out to be necessary. The corner layer is found now separated from the far-field boundary layers by an intermediate viscous layer on each of its sides (see figure 3), all layers being three-dimensional in nature. Specifically, both spanwise length and crossflow velocity scales in the intermediate layers are $O(\delta)$, with $1 \ll \delta \ll Re^{-1/2}$. The far-field boundary layers are considered in § 4, and found to belong to a class of viscous flows developing on swept flat surfaces. In § 5, we turn to investigate boundary layers corresponding to almost planar corners for which similarity-type solutions are derived and found to be non-unique in the parameter space; flow properties reported by Smith (1975) for three-dimensional stagnation point flow into almost planar convex and concave corners are confirmed and generalized to an arbitrary streamwise pressure gradient. Important differences between concave and convex corner flow regimes are then revealed in §§ 6 and 7, respectively, with associated computational difficulties analysed and numerical results presented for both cases. In particular, the corner-layer motion for the latter regime turns out to be mainly controlled by the crossflow. Finally, the special case of viscous flow past a quarter-infinite flat plate is treated in § 8 and compared to the work of Stewartson (1961) with length scales and flow properties being further clarified and elucidated. The most interesting result in the present work appears to be the formation of symmetrically disposed vortices proceeding from the forward corner (depicted in figures 5*b*, 14*b*, 17*b* and suggested by 20) and developing in the intermediate viscous layer. This result was predicted by Moore (1956) by conjectural considerations, but has remained unconfirmed in the literature so far. Our conclusions are given in § 9.

After the first submission of this paper a number of directly/indirectly related works (to corner flows) have appeared in the literature. Most notably Duck, Stow & Dhanak (1999, 2000) have studied non-similarity solutions to the corner boundary-layer equations, and the related boundary-layer flow along a ridge. We note too the very recent work of Duck & Dry (2001) on (unsteady) three-dimensional disturbances to boundary-layer flows, which is also related in some respects to corner flows. Questions of relevances between their works and ours will briefly be considered/discussed where appropriate.

2. The potential flow

2.1. *Posing the problem*

The corner is formed by joining two similar quarter-infinite unswept wedges joined along a side-edge coinciding with Oz (in Cartesian coordinates (x^*, y^*, z^*) and (x, y, z) with $z = z^*$), with the origin taken at the corner vertex and one of the corner walls lying along $y = 0$; the cross-section thus formed varies then with z as illustrated in figure 1. The leading edges of both wedges are kept coplanar and so aligned to an incoming uniform steady stream (of an incompressible fluid) to ensure symmetry with respect to the corner bisector plane, $x^* = 0$. The corner angle is $(\pi - 2\alpha)$ and the opening angle of each wedge is $\alpha_w = \beta\pi$ where $\beta = 2m/(m+1)$ with m being an arbitrary constant.

Our immediate objective is to seek a velocity potential $\Phi(x^*, y^*, z^*)$ satisfying

$$\nabla^2 \Phi = 0, \tag{2.1}$$

$$\frac{1}{r}\frac{\partial \Phi}{\partial \theta} = 0 \quad \text{at} \quad \theta = 0, \quad \theta = \pi - 2\alpha \text{ with } z > 0, \tag{2.2}$$

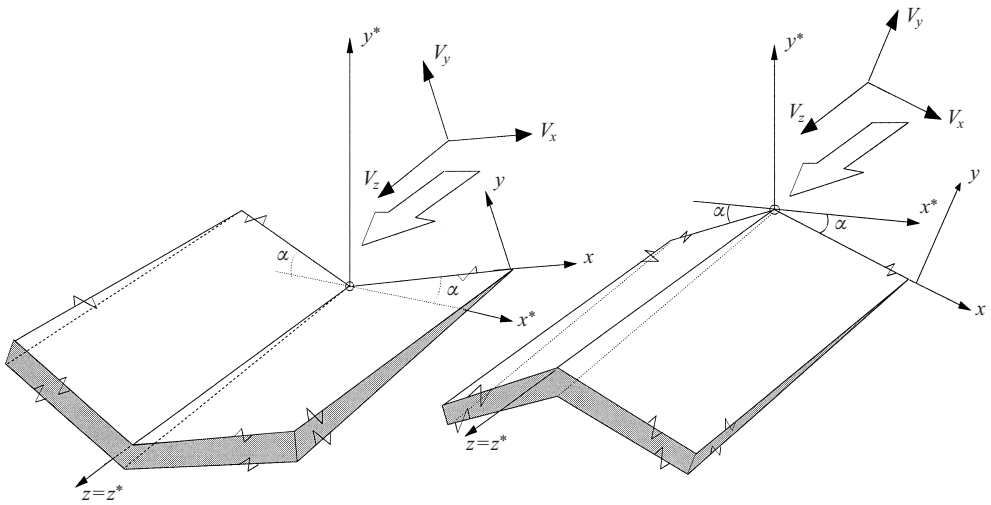

FIGURE 1. Definition sketch of the three-dimensional corner flow configuration showing Cartesian systems (x^*, y^*, z^*) and (x, y, z), to the latter of which is associated the potential flow velocity vector (V_x, V_y, V_z).

together with the usual two-dimensional flow solutions corresponding to each wedge

$$\Phi \sim C z^{m+1} \left[\frac{1}{1+m} - \frac{m}{2} \frac{(r\theta_R)^2}{z^2} \right] + \cdots \quad \text{as} \quad r \to \infty \text{ with } r\theta_R = O(1), \tag{2.3}$$

$$\Phi \sim C z^{m+1} \left[\frac{1}{1+m} - \frac{m}{2} \frac{(r\theta_L)^2}{z^2} \right] + \cdots \quad \text{as} \quad r \to \infty \text{ with } r\theta_L = O(1), \tag{2.4}$$

in which $(x, y) = r(\cos\theta, \sin\theta)$, ∇^2 denotes the three-dimensional Laplacian operator, C is a constant, $\theta_R = \theta \ll 1$, and $\theta_L = \pi - 2\alpha - \theta \ll 1$.

We begin by considering solutions due to Smith (1975) for $m = 1$, and Ridha (1990) for an arbitrary value of m which suggest that problem (2.1)–(2.2) is satisfied by the following asymptotic solution

$$\Phi \sim U_1 z^{m+1} \left[\frac{1}{1+m} - \frac{m}{4} \left(\frac{r}{z} \right)^2 + O\left(\left(\frac{r}{z} \right)^4 \right) \right], \tag{2.5}$$

(with $(r/z) < 1$), but leaves conditions (2.3) and (2.4) unsatisfied, U_1 being an arbitrary constant. We may attempt to resolve this incompatibility by adding correction terms $\tilde{\Phi}(x^*, y^*, z^*)$ (satisfying the Laplace equation together with appropriate boundary conditions) to each of solutions (2.3), (2.4) and (2.5). This suggests that the sought solution may be constructed in the form of an asymptotic representation for each region shown in figure 2 while at the same time noting that the solution of region IV can readily be deduced from that of region II as a consequence of symmetry with respect to the corner bisector plane $x^* = 0$, the intermediate strip III enabling us to match both regions. Note that this construction is crucially different from the traditional one-region approach employed by Rubin (1966) for the zero streamwise pressure gradient case, or the two-region treatment used by Smith (1975) for the three-dimensional stagnation point flow into a corner.

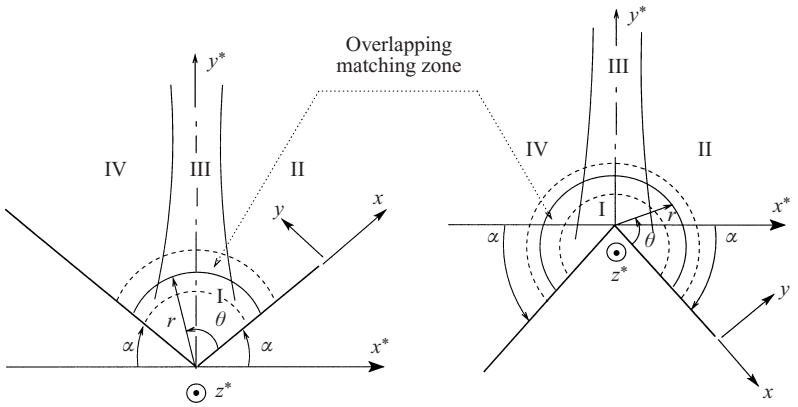

FIGURE 2. A cross-section showing potential flow structure in the vicinity of the corner.

2.2. *Flow regions*

2.2.1. *Region I*

Let $\tilde{\Phi}_1$ be the correction term to be added to solution (2.5) in this region and satisfying

$$\left.\begin{aligned} \nabla^2\tilde{\Phi}_1 &= 0, \\ \frac{1}{r}\frac{\partial\tilde{\Phi}_1}{\partial\theta} &= 0 \text{ at } \theta = 0, \quad \theta = \pi - 2\alpha, \end{aligned}\right\} \tag{2.6}$$

for $z > 0$ with $r/z < 1$. A close examination of (2.5) suggests that we may formally write $r/z = \delta_1 r_1$ and seek the solution of system (2.6) with $\tilde{\Phi}_1 \mapsto z^q\tilde{\Phi}_1(r_1, \theta; \delta_1)$; here, r_1 is $O(1)$ with $\delta_1 \ll 1$ providing a measure for the size of region I whilst q is a constant to be determined. Crucially, (2.5) tells us then that the radial velocity component in this region is also $O(\delta_1)$.

We find

$$\Phi_1 = U_1 z^{1+m}\left(\frac{1}{1+m} - \frac{m}{4}\delta_1^2 r_1^2\right) + \delta_1^2 A z^q r_1^s \cos(s\theta) + O(\delta_1^3), \tag{2.7}$$

for the velocity potential in region I, where $s = 2\pi/(\pi - 2\alpha)$ and A is a constant to be determined together with q from the matching requirements with regions II and III.

2.2.2. *Region II*

In both regions II and IV we are looking for the flow readjustment as region I is approached therefrom, which is equivalent to seeking the effect of one wedge on the velocity potential of the other if it were alone. Now since for two-dimensional flow past a wedge the velocity potential is of the form $U_2 R^k \cos(k\Theta)$, boundary conditions on both wedge walls must be considered; here, U_2 and k are arbitrary constants and (x, R, Θ) is a cylindrical polar coordinate system in which $(y, z) = R(\sin\Theta, \cos\Theta)$. To account for the perturbation effect (represented by $\tilde{\Phi}_2$, say) of the other wedge, we formally introduce the small parameter δ_2 by setting

$$x/R = \delta_2\tilde{x}, \quad \tilde{x} = O(1), \tag{2.8}$$

and so, close to the inner limit of region II, the solution Φ (denoted by Φ_2 in this region) may be sought in the following form

$$\Phi_2 = \{U_2 R^k + \delta_2^2\tilde{\Phi}_2(R, \tilde{x}; \delta_2)\}\cos(k\Theta) \quad \text{for} \quad z > 0, \tag{2.9}$$

in which the first term suggests $\tilde{\Phi}_2 \mapsto R^n \tilde{\Phi}_2(\tilde{x}; \delta_2)$. This leads to

$$\Phi_2 = \{U_2 R^k + \delta_2^2 B R^n \tilde{x}\} \cos(k\Theta) + O(\delta_2^3), \tag{2.10}$$

where n and B are constants to be determined from the matching requirements.

2.2.3. *Region III*

This strip is confined to the neighbourhood of the corner bisector plane and is destined to absorb asymptotically the incompatibility of regions II and IV. The effect of the corner walls on this region is accounted for through the match with either of these two regions or with region I and should consequently be symmetric with respect to the plane $x^* = 0$. This suggests that the appropriate coordinate system here is (x^*, y^*, z^*), as shown in figure 1 and 2, but nonetheless it proves more practical to express the result in the hybrid cylindrical polar coordinates systems, namely (r, θ, z) and (x^*, R^*, Θ^*), with $(y^*, z^*) = R^*(\sin\Theta^*, \cos\Theta^*)$. Again, we seek flow properties for small r/z and so we set $r/z = r_3\delta_3 \ll 1$, with $r_3 = O(1)$, δ_3 being a small parameter. Consistent with the above discussion we find

$$\Phi_3 = U_3 R^{*t} \cos(t\Theta^*) + \delta_3^2 A^* z^a r_3 \sin(\alpha + \theta) + O(\delta_3^3), \tag{2.11}$$

in which the constants U_3, t, a and A^* are to be determined from the matching requirements.

2.3. *Matching*

Thus far, we have derived a particular asymptotic description for each region, namely equations (2.7), (2.10) and (2.11). Our immediate aim now is to show that they match each other in the sense of matched asymptotic expansions as given, for instance, in Van Dyke (1975). For brevity, we shall proceed to match expansions (2.7) and (2.10) in some detail, then match (2.7) and (2.11) but with details omitted. Throughout, z is kept fixed and positive.

We start by considering region II, where it is readily seen that approaching I from II while keeping θ fixed requires $r \to 0$. This implies having $\Theta \to 0$ since $\tan\Theta = y/z$ and so

$$\Phi_2 \sim U_2 R^k + \delta_2^2 B R^n \tilde{x} + O(\Theta^2) + O(\delta_2^3), \tag{2.12}$$

in this limit. Next, approaching II from I while keeping Θ small and fixed (implying keeping $y = r\sin\theta$ small and fixed) requires making r sufficiently large (which is consistent with condition (2.3)) and subsequently we must have $\theta \ll 1$. This coupled to the definitions of the coordinate systems leads to having $\Theta/\theta \sim \delta_1$ in the matching zone and thus yields

$$\Phi_1 \sim U_1 z^{1+m} \left[\frac{1}{1+m} - \frac{m}{4}\delta_1^2 r_1^2\right] + \delta_1^2 z^q r_1^s A + O(\theta^2\delta_1^2), \tag{2.13}$$

for r sufficiently large and $\theta \ll 1$.

To match Φ_1 and Φ_2, solution (2.12) is re-expressed first in function of the variables of region I followed by expanding the different terms in powers of δ_1. We find

$$\Phi_2 = U_2 z^k + \delta_2\delta_1 B z^n r_1 + O(\delta_2\delta_1\theta^2). \tag{2.14}$$

Expressions (2.13) and (2.14) suggest that the match requires having $k = m + 1$, $U_2 = U_1/(1+m)$ and $\delta_1 = \delta_2$ ($= \delta$, say). It is clear now that the match may be made plausible if the terms $z^{1+m}r_1^2$, $z^q r_1^s$ and $z^n r_1$ satisfy an equivalence relationship

of the form

$$\lim_{r_1 \to r_m(z)} \frac{z^{1+m} r_1^2}{z^n r_1} \sim \lim_{r_1 \to r_m(z)} \frac{z^n r_1}{z^q r_1^s} \sim 1, \tag{2.15}$$

for all (admissible) values of m and s, where $r_m(z)$ is to be specified shortly. This suggests that the match may finally be brought to its own conclusion in an overlapping zone for which $r = r_o(z)$ with $r_o/z \ll 1$. To this end, we pose

$$r_0 = l\delta \left(\frac{z}{l}\right)^b, \quad \epsilon\varrho = \ln \frac{r}{r_0}, \tag{2.16}$$

and so $r_m(z) = (z/l)^{b-1}$ in which b is a constant to be determined/fixed, as will be shown later, and ϱ is $O(1)$ with the small parameter ϵ serving to provide a measure, in order of magnitude, for the size of the overlapping zone through

$$\frac{r}{r_0} \sim 1 + \epsilon\varrho + \tfrac{1}{2}\epsilon^2\varrho^2 + \cdots, \tag{2.17}$$

as $r \to r_0$; the quantity l appearing in (2.16) represents a length scale introduced so that r_0 is measured in length units and so it is set to unity in what follows. Accordingly, the equivalence relationship (2.15), together with (2.16), now leads to

$$(1 + m) + 2(b - 1) = n + (b - 1) = q + s(b - 1). \tag{2.18}$$

In the final step of the match we need only ensure matching of the crossflow velocity components in regions I and II, since the streamwise components have already been matched through the zeroth-order terms in δ. To this end, $\partial\Phi/\partial x$ and $\partial\Phi/\partial y$ are first computed from (2.7) and (2.10), and their asymptotic forms are then worked out in the following steps analogous to those leading to (2.13) and (2.14). We find

$$\frac{\partial\Phi_1}{\partial x} \sim -\tfrac{1}{2}\delta m U_1 z^m r_1 + \delta s A z^{q-1} r_1^{s-1} + O(\delta\theta^2), \tag{2.19}$$

$$\frac{\partial\Phi_1}{\partial y} \sim -\tfrac{1}{2} m U_1 y z^{m-1} - s(s-1) A y z^{q-2} r_1^{s-2} + O(\delta\theta^2), \tag{2.20}$$

for region I, and

$$\frac{\partial\Phi_2}{\partial x} \sim \delta B z^{n-1} + O(\delta\Theta^2), \tag{2.21}$$

$$\frac{\partial\Phi_2}{\partial y} \sim -m U_1 y z^{m-1} + O(\delta\Theta^2), \tag{2.22}$$

for region II. Secondly, definitions (2.16) are inserted into (2.19) and (2.20), followed by expanding terms in (r/r_o) in powers of ϵ as in (2.17). Finally, identifying terms of the same order in the resulting equations yields

$$A = \frac{m}{2s(s-1)} U_1, \quad B = \frac{m(2-s)}{2(s-1)} U_1, \tag{2.23}$$

to the leading order in δ. It remains now to match (2.7) with (2.11), following similar steps as for (2.7) and (2.10), but this time with $|\theta + \alpha - \frac{1}{2}\pi| \ll 1$ in view of having region III confined to the immediate neighbourhood of the plane of symmetry. To this end, we note that approaching I from III requires having $\Theta^* \ll 1$ since $y^*/z^* \ll 1$. This results in

$$\begin{aligned} &\delta_3 = \delta, \quad t = m + 1, \quad a = m + b, \\ &A^* = -B, \quad U_3 = U_1/(1 + m). \end{aligned} \tag{2.24}$$

Accordingly, we find for region I

$$V_x = \delta U_1 z^{m+b-1}\left[-\tfrac{1}{2}m\left(\frac{x}{r_0}\right) + \frac{m}{2(s-1)}\left(\frac{r}{r_0}\right)^{s-1}\cos(s-1)\theta\right], \tag{2.25}$$

$$V_y = \delta U_1 z^{m+b-1}\left[-\tfrac{1}{2}m\left(\frac{y}{r_0}\right) - \frac{m}{2(s-1)}\left(\frac{r}{r_0}\right)^{s-1}\sin(s-1)\theta\right], \tag{2.26}$$

$$V_z = U_1 z^m, \tag{2.27}$$

to the leading order of approximations in δ, where (V_x, V_y, V_z) are the inviscid flow velocity components associated with the Cartesian coordinates frame (x, y, z). Similarly, we find close to the inner limit of region II

$$V_x = \delta\frac{m(2-s)}{2(s-1)}U_1 R^{m+b-1}\cos(k\Theta), \tag{2.28}$$

$$V_y = -U_1 R^m \sin(m\Theta), \tag{2.29}$$

$$V_z = U_1 R^m \cos(m\Theta), \tag{2.30}$$

to the leading order of approximations in δ, which are readily seen to be analogous to potential flow velocity components past a swept wedge.

There are two key observations to be made at this stage. The first concerns the quantity δ (or equivalently δ_i, $i = 1, 2, 3$). In conformity with potential flow theory, δ must be greater than the boundary-layer thickness, that is $\delta \gg Re^{-1/2}$. On account of this estimation, it is readily deduced from solutions (2.25)–(2.30) that the coupling created by the mutual interaction of inviscid flows on the corner walls gives rise to a crossflow an order of magnitude greater (specifically in the corner-line vicinity) than that found by Rubin (1966) due to the boundary-layer displacement effect, which is $O(Re^{-1/2})$, where $Re = LU_\infty/\nu$, a characteristic Reynolds number, is assumed to be large, with U_∞ and L denoting typical velocity and length scales in the streamwise direction, ν being the kinematic viscosity. Obviously, this is a fundamental difference in order of magnitudes which will prove to be crucial in finding viscous regions and flow characteristics, hitherto unsuspected, in concave and convex corners alike, as shown in § 3 and in later sections.

Secondly, the quantity b appearing in solutions (2.25)–(2.30), which remained thus far undetermined, appears to be arbitrary and expresses thus the generic nature of these corner flow solutions. Of particular interest here is the case $b = \frac{1}{2}(1-m)$ for which boundary-layer equations admit self-similar solutions. Subsequently, the matching requirement (2.18) can be written in the form†

$$\tfrac{1}{2}(1+m) = q/s = n/1 \tag{2.31}$$

in which the respective terms represent ratios between the powers of z and r_1 appearing in $z^{1+m}r_1^2$, $z^q r_1^s$ and $z^n r_1$ of (2.13) and (2.14).

In line with the above discussion, we will here devote our attention to steady laminar incompressible boundary-layer flow along a corner of arbitrary angle, obtained when

† In the first version of this paper relation (2.31) was intuitively deduced, and used as a matching requirement instead of the more general equivalence relationship (2.15), and its consequence (2.18), which were both absent therefrom.

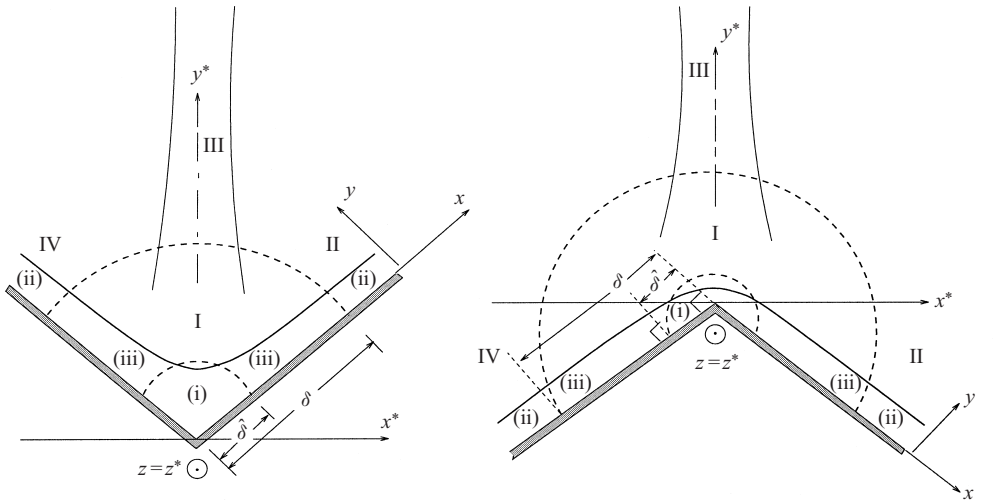

FIGURE 3. A sketch illustrating the structure of three-dimensional viscous layers in the corner vicinity: zone (i) is obtained when $r \to 0$, $\theta \sim 1$, (ii) for r large and θ small with $r\theta \sim Re^{-1/2}$, (iii) is the blending intermediate layer.

$b = \frac{1}{2}(1 - m)$. We start by general considerations of the viscous motion in zones adjacent to I, II and IV.

3. Boundary-layer structure and approximations

One of the key elements of the matching requirements of the potential flow regions I and II (discussed in § 2.3) lies in the order of magnitude estimation $\Theta/\theta \sim \delta$ (with $\delta \gg Re^{-1/2}$), which, when coupled to boundary-layer considerations, leads to dividing the viscous motion into five distinct regions (or three when symmetry is taken into account) as depicted in figure 3. Here, region (i) represents the usual corner layer which is fully three-dimensional whilst (ii) mirrors primarily a boundary-layer motion on a wedge with a crossflow in the x-direction. Accordingly, the intermediate boundary layer, namely region (iii), must then be allowed to merge smoothly with the previous ones at its inner and outer limits, respectively. It is specifically this layer that constitutes the genesis of this new structure, particularly its spanwise velocity and length scales, which are both $O(\delta)$. That is why the present viscous flow structure is crucially different from the traditional three-region one introduced by Rubin (1966) (and adopted later by other authors) for the zero streamwise pressure gradient situation.

To analyse the viscous motion in each of these regions we introduce the following boundary-layer scaled variables

$$\left.\begin{array}{lll} X = x/L\delta_x, & Y = y/L\delta_y, & \hat{z} = z/L, \\ \hat{U}(X,Y,\hat{z}) = v_x/U_\infty\varepsilon_x, & \hat{V}(X,Y,\hat{z}) = v_y/U_\infty\varepsilon_y, & \hat{W}(X,Y,\hat{z}) = v_z/U_\infty, \\ \hat{P}(X,Y,\hat{z}) = p/\rho U_\infty^2, & (\delta_y,\varepsilon_x,\varepsilon_y) \ll 1, & \end{array}\right\} \quad (3.1)$$

where (v_x, v_y, v_z) are the viscous flow velocity components associated with the (x, y, z)-directions, p is the pressure, $L(\delta_x, \delta_y, 1)$ and $U_\infty(\varepsilon_x, \varepsilon_y, 1)$ are characteristic length and velocity scales such that $\hat{U}$, $\hat{V}$, $\hat{W}$ and $\hat{P}$ are $O(1)$; for convenience the hat symbol $\hat{}$ will hereinafter be dropped from z. To derive boundary-layer equations for

each viscous region, first, definitions (3.1) are inserted into the Navier–Stokes and continuity equations, then boundary-layer approximations are carried out subject to the potential flow constraints, equations (2.25)–(2.30); in view of symmetry, we need only consider then the space defined by $z > 0$ and $\alpha + \theta \leqslant \frac{1}{2}\pi$.

In the corner-layer, region (i), boundary-layer approximations require that forces due to the viscous interaction with both surfaces must, in general, be of the same order of magnitude. This amounts to having

$$\delta_x \sim \delta_y = \hat{\delta}, \tag{3.2}$$

and subsequently $\varepsilon_x \sim \varepsilon_y$ ($= \varepsilon$, say) from continuity considerations, leading to

$$\hat{U} \sim \hat{\delta}\varepsilon^{-1}\{1 + O((\hat{\delta}/\delta)^{s-2})\}, \tag{3.3}$$

according to (2.25), which must be $O(1)$. Now since $\hat{\delta} \ll \delta$, it follows that two distinct situations exist depending upon whether $s > 2$ or $1 < s < 2$ which must then be joined by a 'matching' situation when $s \sim 2$, i.e. $|\alpha| \ll 1$; such a situation corresponds to almost planar corners. Additionally, the case $s = 1$, corresponding to the quarter-infinite flat-plate problem, gives rise to a singularity and therefore requires a special treatment. From our boundary-layer order of magnitude analysis, the following picture emerges:

$$\text{region (i)} \quad \begin{cases} \text{concave corners, } s > 2: & \hat{\delta} = Re^{-1/2},\ \varepsilon = Re^{-1/2}, \\ \text{convex corners, } s < 2: & \hat{\delta} = Re^{-1/s}\delta^{(s-2)/s},\ \varepsilon = Re^{(1-s)/s}\delta^{(2-s)/s}, \end{cases} \tag{3.4}$$

$$\text{region (iii) } s \geqslant 1, \text{ but } s \neq 2: \quad \delta_x = \varepsilon_x = \delta,\ \delta_y = \varepsilon_y = Re^{-1/2}, \tag{3.5}$$

$$\text{region (ii) } s \geqslant 1, \text{ but } s \neq 2: \quad \delta_x \gg \delta,\ \varepsilon_x = \delta,\ \delta_y = \varepsilon_y = Re^{-1/2}. \tag{3.6}$$

Regarding the semi-infinite flat plate limit, it will shortly be shown in § 5 that:

$$s \to 2 \quad \begin{cases} \text{region (i)}: & \hat{\delta} = Re^{-1/2},\ \varepsilon = Re^{-1/2}, \\ \text{region (iii)}: & \delta_x = \delta,\ \varepsilon_x = \delta/\ln Re,\ \delta_y = \varepsilon_y = Re^{-1/2}, \\ \text{region (ii)}: & \delta_x \gg \delta,\ \varepsilon_x = \delta/\ln Re,\ \delta_y = \varepsilon_y = Re^{-1/2}. \end{cases} \tag{3.7}$$

Questions related to the limit $s \to 1$ will be tackled in § 8.

It is clear now that different dominant flow characteristics may be expected in each region, for concave and convex corners alike, and they must be considered separately. For clarity as well as for convenience, we shall start by examining first the boundary layer in region (ii).

4. The outer layer: region (ii)

Here, the order of magnitude estimations, (3.6), lead to the following boundary-layer equations:

$$\hat{V}\hat{U}_Y + \hat{W}\hat{U}_z = -\delta^{-2}\hat{P}_X + \hat{U}_{YY}, \tag{4.1}$$

$$\hat{P}_Y = O(Re^{-1}), \tag{4.2}$$

$$\hat{V}\hat{W}_Y + \hat{W}\hat{W}_z = -\hat{P}_z + \hat{W}_{YY}, \tag{4.3}$$

$$\hat{V}_Y + \hat{W}_z = 0. \tag{4.4}$$

These are to be solved subject to $\hat{U} = \hat{V} = \hat{W} = 0$ on the wall, together with the potential flow constraints, equations (2.28)–(2.30), as $Y \to \infty$. Equations (4.1)–(4.3) suggest setting $\hat{P} = P_0(z) + \delta P_1(X, z) + \delta^2 P(X, z) + \cdots$.

To obtain similarity solutions we introduce the following transformations

$$\left.\begin{aligned} \psi(Y, z) &= cz^{(m+1)/2} f(\eta),\ \hat{U}(Y, z) = Bz^{(m-1)/2} g(\eta), \\ \hat{P}(X, z) &= -\tfrac{1}{2} z^{2m}[1 + \delta^2 (m-1) z^{-(1+m)/2} BX + \cdots], \end{aligned}\right\} \tag{4.5}$$

where $\hat{W} = \psi_Y$, $\hat{V} = -\psi_z$, $\eta = z^{(m-1)/2} Y/c$, $B = m(2-s)/2(s-1)$, and $c = \sqrt{2/(1+m)}$. Inserting these into equations (4.1)–(4.4) yields

$$g'' + fg' + (\beta - 1)(1 - f'g) = 0, \tag{4.6}$$

$$f''' + ff'' + \beta(1 - f'^2) = 0, \tag{4.7}$$

subject to

$$\left.\begin{aligned} f = g = f' = 0 \quad &\text{at} \quad \eta = 0, \\ f' \to 1,\ g \to 1 \quad &\text{as} \quad \eta \to \infty, \end{aligned}\right\} \tag{4.8}$$

in which $(\,.\,)' = \mathrm{d}(\,.\,)/\mathrm{d}\eta$. For brevity, numerical results for this region are given and discussed with those of the intermediate layer since they provide boundary conditions for it.

5. Boundary layer in almost planar corners

For this situation, we clearly have $|s-2| \sim 4|\alpha|/\pi \ll 1$. Should we now consider the potential flow constraints (namely, equations (2.25) and (2.26)) as $r \to Re^{-1/2}$ it would easily be seen (as in Smith 1975) that the resulting asymptotic form thereof remains valid (in this limit) if $\alpha \sim O(1/\ln Re)$ or smaller. The fact that $1 \gg \delta \gg Re^{-1/2}$ suggests setting $\delta = O(Re^{-1/M}), M > 2$ (or $\delta \sim Re^{-1/2} \ln Re$), and so we may write

$$\alpha = \frac{K}{\ln Re} \quad (K \sim 1), \tag{5.1}$$

as $s \to 2$. With this estimation, we can move on now to investigating flow characteristics in regions (iii) and (i).

5.1. *The intermediate layer: region* (iii)

5.1.1. *Governing equations*

According to the above discussion, (2.25) and (2.26) reveal that region (iii) is characterized by $\varepsilon_x = \delta/\ln Re$ for $s \sim 2$, together with $\varepsilon_y = \delta_y = Re^{-1/2}$, and $\delta_x = \delta$ in view of boundary-layer approximations. These scales lead to a set of boundary-layer equations as (4.1)–(4.4) but now with $\delta^{-2} \ln Re$ replacing δ^{-2} in (4.1), and so similarity solutions can be obtained by introducing the following variables

$$\left.\begin{aligned} \psi_1(X, Y, z) &= cz^{(m+1)/2} \left[f(\eta) + \frac{K}{\ln Re} f_1(\xi, \eta) + \cdots \right], \\ \hat{U}(X, Y, z) &= \frac{2m}{\pi} K \xi (\ln \xi - 1) z^{(m-1)/2} g_1(\xi, \eta), \end{aligned}\right\} \tag{5.2}$$

where $\hat{W} = \psi_{1Y}$, $\hat{V} = -\psi_{1z}$, and $\xi = z^{(m-1)/2} X$. We find

$$g_1'' + fg_1' + \gamma(\xi)(\beta - 1)(1 - f'g_1) = \xi(\beta - 1) f' \frac{\partial g_1}{\partial \xi}, \tag{5.3}$$

$$f''' + ff'' + \beta(1 - f'^2) = 0, \tag{5.4}$$

subject to

$$\left.\begin{aligned} f(0) = f'(0) = g_1(\xi, 0) &= 0, \\ g_1(\xi, \infty) = f'(\infty) &= 1, \\ g_1(1, .) &= g(.), \end{aligned}\right\} \tag{5.5}$$

in which $\gamma(\xi) = (2\ln\xi - 1)/(\ln\xi - 1)$, and $0 < \xi \leqslant 1$ in view of the relevant scalings and definitions. Observe that system (5.3)–(5.5) leads, when $\beta = 1$, to the stagnation point flow solution g_1 found by Smith (1975). Note also that it asymptotes to (4.7)–(4.8) as $\xi \to 1$, which assures matching with region (ii). However, when $\xi \to 0$, the match with region (i) would require an infinite number of terms for reasons similar to those given in (Smith 1975), since, as $r \to Re^{-1/2}$, terms in $(\ln r/r_0)^n$ start to have 'comparable contributions to the main effect' of inviscid–viscous flow interaction.

5.1.2. *Results and discussions*

Equations (5.3)–(5.5) were discretized using the Crank–Nicholson approximation in the ξ-direction and the resulting equations were then solved by an implicit second-order finite differencing scheme. Hereinafter, numerical results will in general be presented in terms of the velocity components $u(\xi,\eta)$, $v(\xi,\eta)$ and $w(\xi,\eta)$:

$$(\hat{U}(X,Y,z), \hat{V}(X,Y,z)) = z^{(m-1)/2}(u(\xi,\eta), v(\xi,\eta)), \;\; \hat{W}(X,Y,z) = z^m w(\xi,\eta), \tag{5.6}$$

and in terms of the streamwise vorticity function $\omega(\xi,\eta) = -u_\eta/c$, as deduced from

$$\left(\frac{\varepsilon_y}{\delta_x}\right)\hat{V}_X - \left(\frac{\varepsilon_x}{\delta_y}\right)\hat{U}_Y \sim \left(\frac{\delta Re^{1/2}}{\ln Re}\right) z^{m-1}\omega, \tag{5.7}$$

to the leading order in Re^{-1} for the present situation. In particular, we will set, without loss of generality, $K = 1$ in this subsection only.

Numerical results are presented in figures 4 and 5. The effect of varying the pressure gradient parameter β on the crossflow shear stress $u_\eta(\xi, \eta = 0)/c$ is illustrated in figure 4. Here, it is seen that $u_\eta(\xi, \eta = 0)/c$ behaves in a non-monotonic fashion with respect to β and tends always to zero as the origin $\xi = 0$ is approached. The corresponding evolution of the velocity profile $u(\xi,\eta)$ is shown in figure 5(a); we observe here that $u(\xi,\eta)$ exhibits, over a portion of the ξ-range, an inflection point for $-0.19884 \lesssim \beta \lesssim 0.706\cdots$, a behaviour that is synonymous with a streamwise crossflow–vortex structure formation. This is shown in figure 5(b) which depicts constant contour lines of the streamwise vorticity function $\omega(\eta,\xi)$; for $0 < \beta < 0.706\cdots$, the vorticity contours show layers of positive (away from the wall) and negative (generated at the wall) vorticity. We see that the vortex lies near the centre of region (iii) for β small, and drifts, with increasing β, downwards towards the wall while moving sideways towards the outer limit $\xi = 1$. Importantly, since the existence of crossflow–vortex structures is known to greatly influence other disturbances (Reed & Saric 1989), this result obviously suggests investigating the corner-flow instability in the intermediate layer proper, and studying its effect on the corner layer, particularly for a small streamwise pressure gradient regime. We note, at this stage, that such a structure was predicted by Moore (1956) (specifically within the corner layer) but has remained unconfirmed in the literature so far. We will see in §§ 6.1.3 and 7.2.3 that such vortices are also generated by flows along concave and convex corners alike, including the quarter-infinite flat-plate limit.

In this flow regime, for almost planar convex corners ($K < 0$), the crossflow pattern in region (iii) is practically a mirror image of that obtained for concave corners and is obviously associated to a closed vortex rotating in the opposite sense.

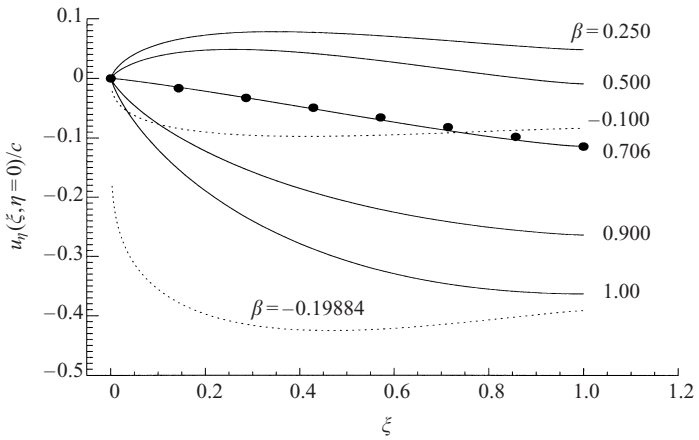

FIGURE 4. Almost planar corners, region (iii): distribution of the x-component of the wall shear stress ($Ku_\eta(\xi,\eta=0)/c$, $K=1$). ●, linear relationship $u_\eta(\xi,\eta=0)/c=-0.114\xi$.

5.2. *The corner layer: region* (i)

5.2.1. *Governing equations*

Here, we have $\delta_x=\delta_y=\varepsilon_x=\varepsilon_y=Re^{-1/2}$. Hence, the boundary-layer equations are

$$\hat{U}\hat{U}_X+\hat{V}\hat{U}_Y+\hat{W}\hat{U}_z=-P_X+\hat{U}_{XX}+\hat{U}_{YY}, \tag{5.8}$$

$$\hat{U}\hat{V}_X+\hat{V}\hat{V}_Y+\hat{W}\hat{V}_z=-P_Y+\hat{V}_{XX}+\hat{V}_{YY}, \tag{5.9}$$

$$\hat{U}\hat{W}_X+\hat{V}\hat{W}_Y+\hat{W}\hat{W}_z=-P_{0z}+\hat{W}_{XX}+\hat{W}_{YY}, \tag{5.10}$$

$$\hat{U}_X+\hat{V}_Y+\hat{W}_z=0, \tag{5.11}$$

in which $\hat{P}=P_0(z)+Re^{-1/2}P_1(X,Y,z)+Re^{-1}P(X,Y,z)+\cdots$.

To derive similarity solutions we pose first $\hat{r}^2=X^2+Y^2$ and use the two-dimensional conformal transformation

$$\left.\begin{aligned}\hat{r}\exp(\mathrm{i}\theta)=cz^{(1-m)/2}\rho^n\exp(\mathrm{i}n\chi)\quad(n=2/s),\\(\tilde{\xi},\tilde{\eta})=\rho(\cos\chi,\sin\chi),\end{aligned}\right\} \tag{5.12}$$

followed by eliminating the pressure gradient terms in the x- and y-directions to obtain the streamwise vorticity equation. This amounts to seeking solutions in the form

$$\hat{U}=-Z\{J^{-1/2}[F\cos(\theta-\chi)-G\sin(\theta-\chi)]+(\beta-1)\rho^nH\cos\theta\}, \tag{5.13}$$

$$\hat{V}=-Z\{J^{-1/2}[F\sin(\theta-\chi)+G\cos(\theta-\chi)]+(\beta-1)\rho^nH\sin\theta\}, \tag{5.14}$$

$$\hat{W}=z^mH,\ \omega=(F_{\tilde{\eta}}-G_{\tilde{\xi}})/J, \tag{5.15}$$

where F, G and H are functions of $(\tilde{\xi},\tilde{\eta})$ only with $J=n^2\rho^{2(n-1)}$ and $Z=c^{-1}z^{(m-1)/2}$; here $(.)_{\tilde{\xi}}$, $(.)_{\tilde{\eta}}$ stand for partial derivatives with respect to $\tilde{\xi}$ and $\tilde{\eta}$, respectively. In what follows, we will drop the tilde from $\tilde{\xi}$ and $\tilde{\eta}$, and refrain, for the sake of brevity, from giving the resulting similarity equations.

The boundary conditions are

$$F=G=H=0\quad\text{at }\eta=0, \tag{5.16}$$

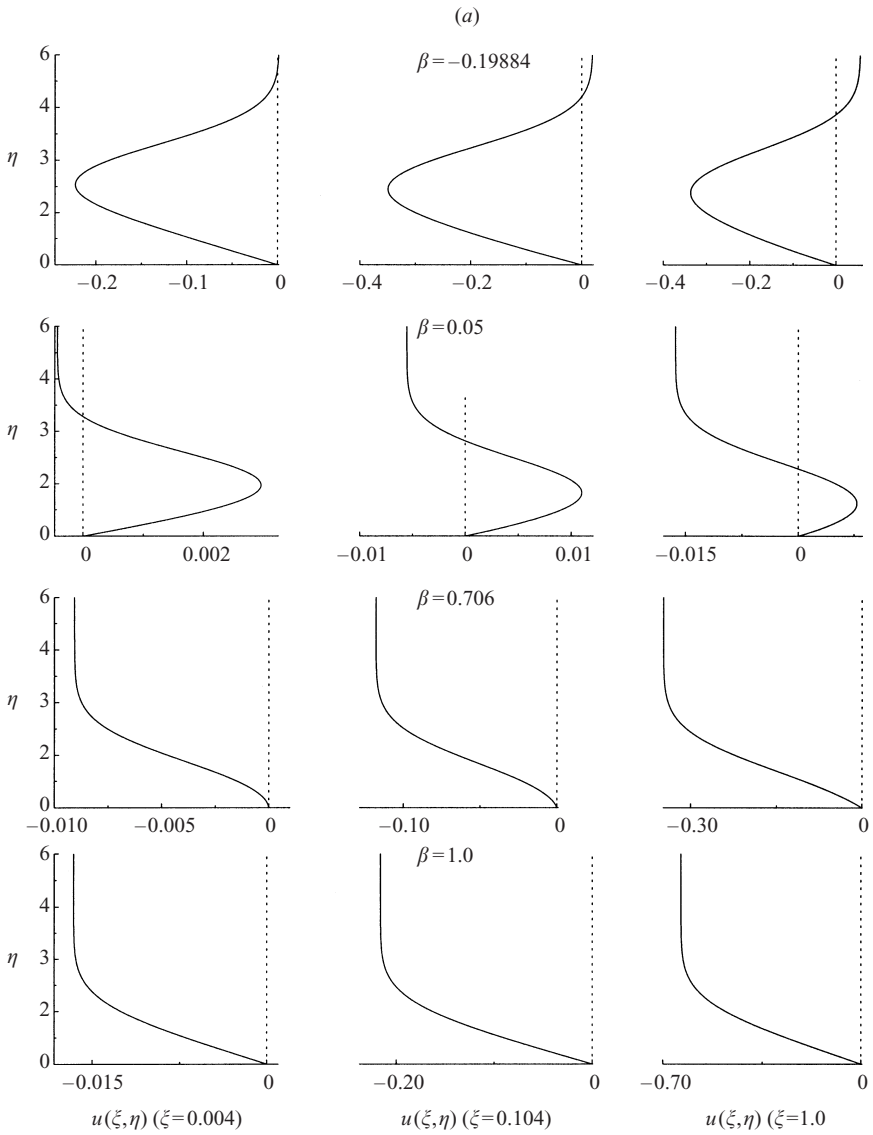

FIGURE 5(*a*). For caption see facing page.

together with

$$\left.\begin{aligned} F &\sim \xi[1-\tfrac{1}{2}\beta(1+\exp(-2K/\pi))]+O(\alpha) \quad \text{for} \quad H\to 1,\\ G_\eta &\sim [1-\tfrac{1}{2}\beta(1-\exp(-2K/\pi))]+O(\alpha) \quad \text{for} \quad \omega\to 0, \end{aligned}\right\} \tag{5.17}$$

as $\eta\to\infty$, in which conditions on F and G have been deduced from (2.25) and (2.26) subject to definitions (5.13) and (5.14) as $s\to 2$, with K replacing $K(M-2)/M$ herein; in deriving these conditions, only terms in $(\delta Re^{1/2})^{2-s}$ have been approximated.

Additionally, symmetry requires

$$H_\xi = G_\xi = F = \omega = 0 \quad \text{at } \xi = 0 \tag{5.18}$$

which, as in Smith (1975), suggests, together with (5.17), looking for solutions in

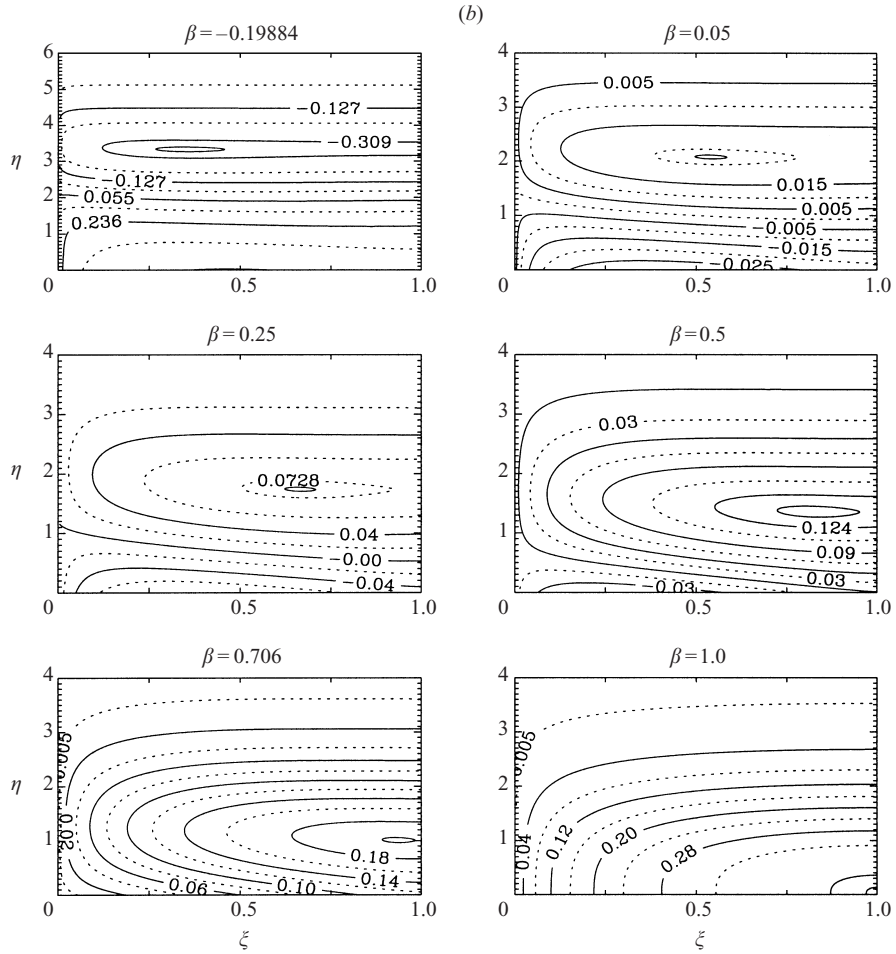

FIGURE 5. Almost planar corner, region (iii): effect of the parameter β on (*a*) the evolution of the crossflow velocity u, and (*b*) the streamwise vorticity ω.

the form

$$(F, G, H, \omega)(\xi, \eta) = (\xi F_0, G_0, H_0, \xi\omega_0)(\eta) + (F_1, G_1, H_1, \omega_1)(\xi, \eta)/\ln Re + \cdots . \quad (5.19)$$

Substituting (5.19) into the governing equations of the similarity solutions yields

$$H_{0\eta\eta} + G_0 H_{0\eta} + \beta(1 - H_0^2) = 0, \quad (5.20)$$

$$\omega_{0\eta\eta} + G_0\omega_{0\eta} + [F_0 + (2-\beta)H_0]\omega_0 - 2(1-\beta)H_0 H_{0\eta} = 0, \quad (5.21)$$

$$F_0 + G_{0\eta} - (2-\beta)H_0 = 0, \quad (5.22)$$

$$\omega_0 - F_{0\eta} = 0, \quad (5.23)$$

to the leading order in Re^{-1}. The boundary conditions are

$$\left.\begin{aligned} F_0 = G_0 = H_0 = 0 \quad \text{at } \eta = 0, \\ F_0 \to 1 - \tfrac{1}{2}\beta(1 + \exp(-2K/\pi)), \quad H_0 \to 1, \ \omega_0 \to 0 \quad \text{as } \eta \to \infty. \end{aligned}\right\} \quad (5.24)$$

System (5.20)–(5.24) fixes primary flow features in region (i), and is in essence the same as that derived by Ridha (1990) for the corner-layer side-edge, and Ridha

(1996) for forced convection flow states. It has also the same form as that derived by Dhanak & Duck (1997, system (3.1)–(3.4), p. 1797), Duck *et al.* (2000) and Duck & Dry (2001), specifically for $K = 0$ but with different conditions as $\eta \to \infty$. Although system (5.20)–(5.24) has been derived for $K \sim 1$, it turns out to be instructive to look into its properties as $|K| \to \infty$. For instance, when $K \to \infty$ we recover the corner-layer side-edge boundary conditions corresponding to concave corner situations. Physically speaking, this implies that flow features at the corner-layer side-edge (or at the inner limit of the intermediate boundary layer) become dominant throughout the corner-layer as $s \to 2$. Indeed, it will be seen later (for concave corners, § 6.1.2) that similarity solutions in the inner limit of region (iii) are governed by a set of equations equivalent to (5.20)–(5.23), in which the governing equation of F_0 can be derived by substituting $\omega_0 = F_{0\eta}$ from (5.23) into (5.21), followed by integrating the result once with respect to η to find

$$F_{0\eta\eta} + G_0 F_{0\eta} + F_0^2 + (\beta - 1)H_0^2 = Q_0, \tag{5.25}$$

after exploiting (5.22) and using boundary conditions at $\eta = 0$, Q_0 being a constant determined by applying the appropriate boundary conditions at $\eta = \infty$.

On the other hand, when K is set identically equal to zero the two-dimensional wedge configuration is recovered, of course, with condition (2.25) (subsequently (5.17)) leading to $\hat{U}(X, Y = \infty, z) = 0$ (subsequently $F(\xi, \eta = \infty) = 1 - \beta$), that is an inviscid flow with a zero crossflow component. One solution of system (5.20)–(5.24) in this particular regime is obviously the classical (two-dimensional) Falkner–Skan solution (Rosenhead 1966) for which $F_0 = (1 - \beta)H_0$. However, there exists a second family of solutions in this regime which is completely three-dimensional in nature. It is our view that this solution family is not linked to a corner flow since $K = 0$ corresponds to $\alpha = 0$. Nevertheless, this solution family is important in its own right for it does represent, for example, a class of boundary-layer flows on swept surfaces and as such deserves more attention. In this connection, see the studies by Duck *et al.* (2000) and Duck & Dry (2001) on three-dimensional boundary-layer flows governed essentially by the same similarity equations, which, in addition, highlight interesting stability aspects thereof, and their possible link to bypass transition.†

System (5.20)–(5.24) has numerically been solved by a fourth-order Runge–Kutta method and non-uniqueness of solutions is found common in the (K, β) parameter space. In this regard, and in view of the above discussions, we find it preferable to consider separately some of their asymptotic features according to the order of magnitude of K; numerical results will be presented in terms of (u_0, v_0, w_0):

$$(u(\xi, \eta), v(\xi, \eta), w(\xi, \eta)) = (\xi u_0(\eta), v_0(\eta), w_0(\eta)) + O(1/\ln Re). \tag{5.26}$$

5.2.2. *The $K = O(1)$ case*

Numerical results are shown in figures 6–9. We shall first focus our attention on the variation of $w_{0\eta}(\eta = 0)$ and $u_{0\eta}(\eta = 0)$ in the (K, β) parameter space; these are depicted in figure 6, with the Blasius point indicated on figure 6(*a*) for reference and completeness. Here, it is generally seen that the solution is non-unique with at least two distinct families of solutions existing over the range of values of (K, β) shown. That is why we find it convenient to refer, hereinafter, to that family of solutions having (for the most part of the β range shown, particularly for $\beta \geqslant 0$) the greatest value of $w_{0\eta}(\eta = 0)$ as the upper solution branch, the other family being referred to now as the lower branch.

† This was brought to our attention by one of the referees.

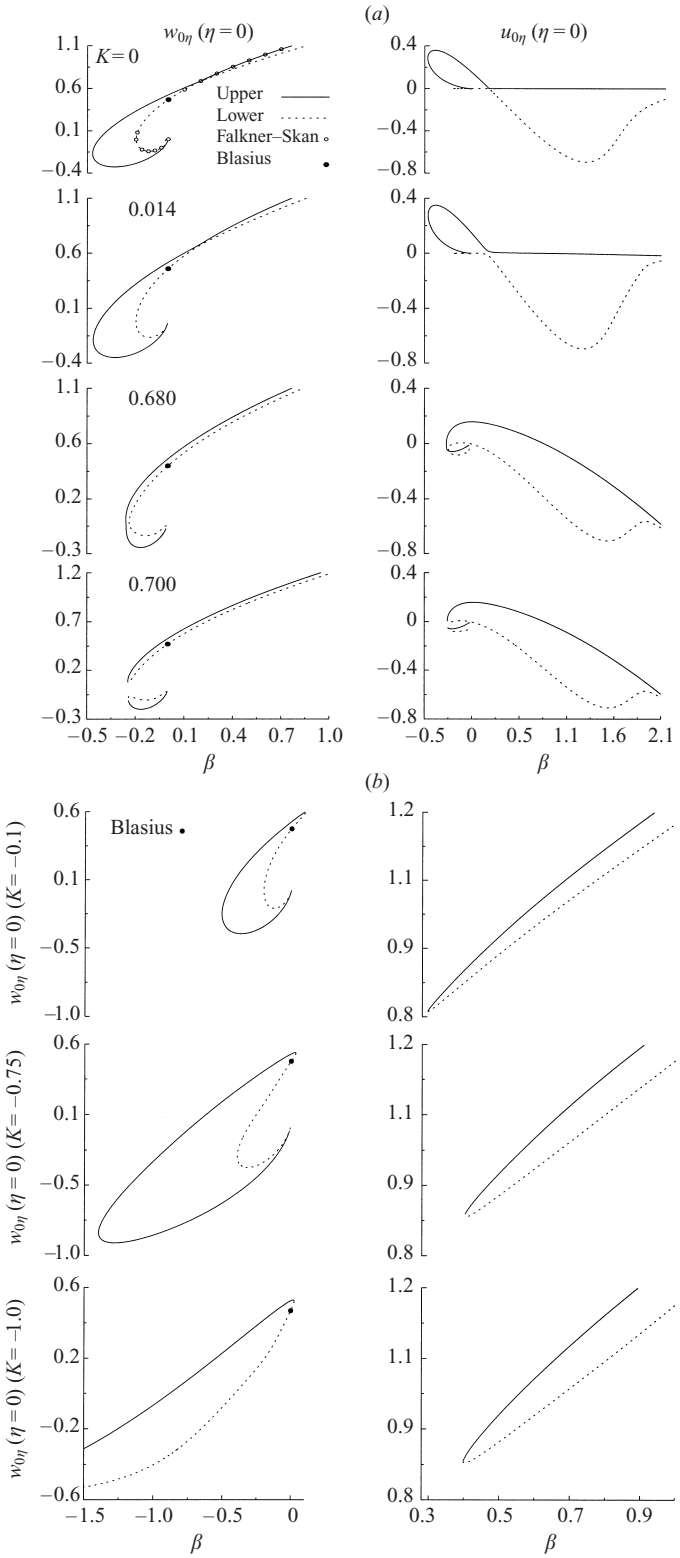

FIGURE 6. For caption see page 241.

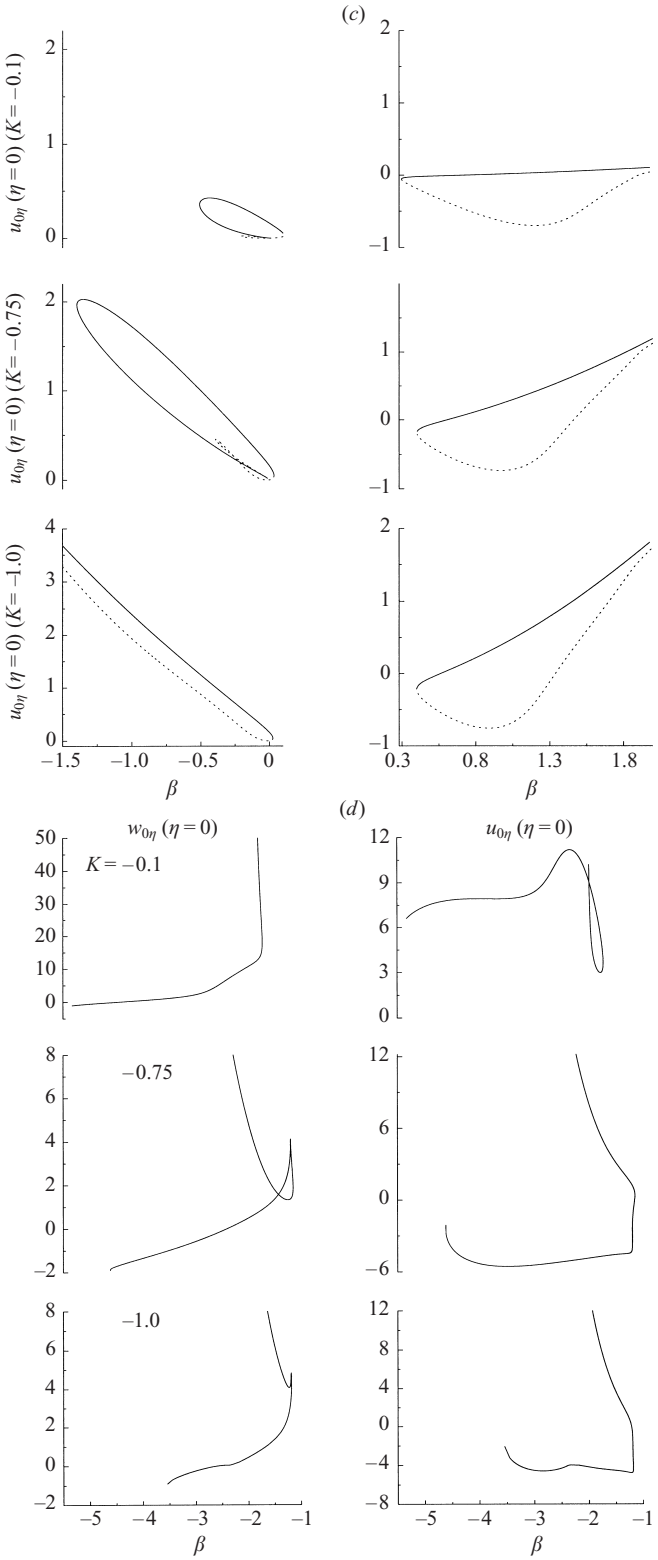

FIGURE 6. For caption see facing page.

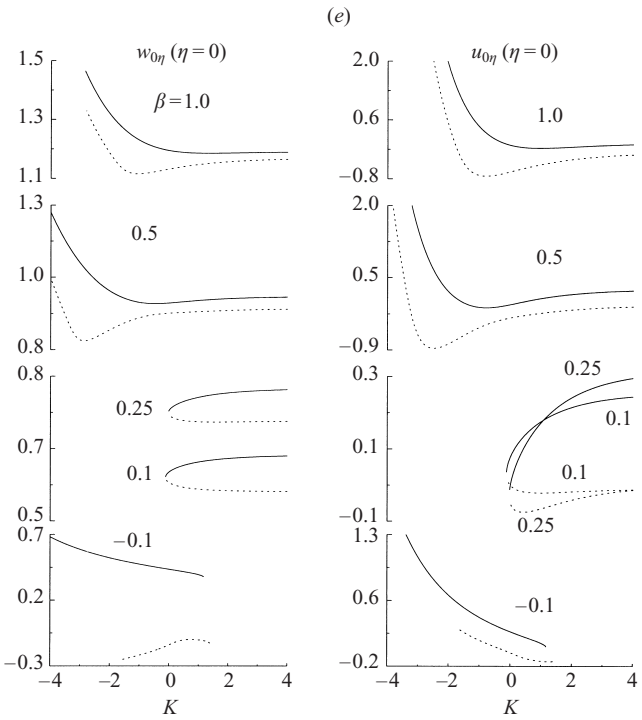

FIGURE 6. Almost planar corners, region (i), with $K \sim O(1)$: $W_{0\eta}(\eta = 0)$ and $U_{0\eta}(\eta = 0)$ distributions with varying β and K, as indicated.

The effect of varying β, with K fixed and positive, is shown in figure 6(a). When $K = 0$, the classical two-dimensional Falkner–Skan solution (identified with $u_0(\eta) = 0$) is found to coincide with the lower branch for $\beta \lesssim 0.1927\ldots$ and with the upper for $\beta \gtrsim 0.1927\ldots$, both branches becoming instantaneously identical when $\beta \simeq 0.1927\ldots$. As K increases, both solution branches become completely three-dimensional in nature, and a small loop solution emerges close to the origin for $K > 0.68$.

Results for $K < 0$ and fixed, with varying β, are illustrated in figures 6(b)–6(d). Here, the main solution branches are seen to split up, over the range of (K, β) shown, into two distinct parts separated by a β-interval for which no solution exists. For $\beta < -1$, a further solution family emerges (see figure 6d) which is apparently not linked to the two main branches extending from the case $K = 0$ (figure 6a). This new solution is characterized by relatively large positive values of $w_{0\eta}(\eta = 0)$, and is associated to an overshoot in the streamwise velocity $w_0(\eta)$ profile (see figure 7c). That is why it will be referred to as the 'overshoot' branch.

Lastly, the effect of varying K, with β fixed, is shown in figure 6e. Here, when β is small and positive, no solution is found to exist for values of K below some small negative value: for example, for $\beta = 0.1$ and 0.25 no solution exists when K is smaller than -0.123 and -0.03, respectively.

We consider now solution profiles for $w_0(\eta)$ and $u_0(\eta)$, a selection of which is presented in figure 7, namely for $K = 0.70$ and -0.75. For the particular case $K = 0$ (figure 7b), profiles for $w_0(\eta)$ belonging to the upper solution branch are generally seen to be reversed for $\beta < -0.4283$ with solutions taking the form of a massively displaced shear layer on the lower portion thereof for $-0.4678 \leqslant \beta \leqslant 0$. For the

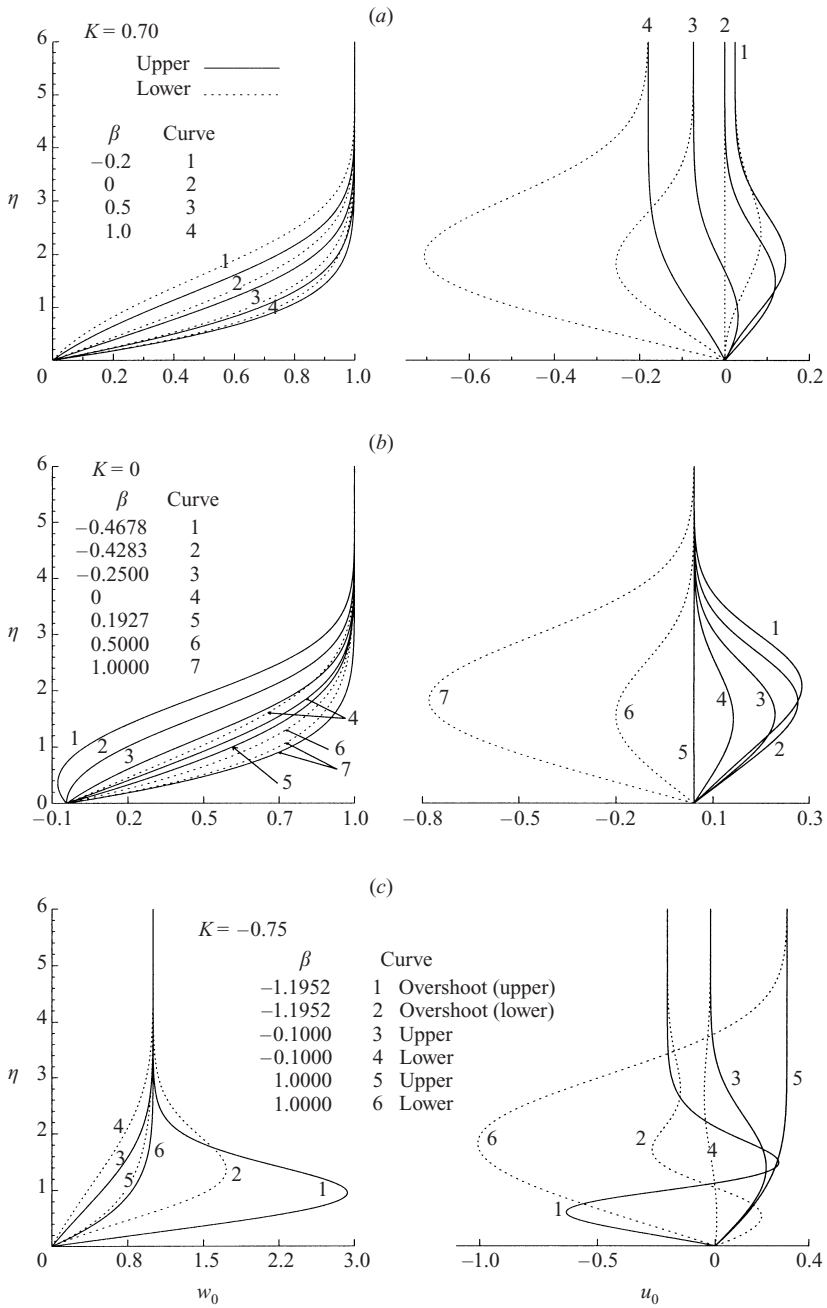

FIGURE 7. Almost planar corners, region (i), with $K \sim O(1)$: w and u profiles for different K-states, β as indicated.

crossflow velocity, we generally see that $u_0(\eta)$ possesses, when $K = 0$, a jet-like profile directed towards the symmetry plane for $\beta > 0.1927\ldots$ and away therefrom for $\beta < 0.1927\ldots$, the case $\beta = 0.1927\ldots$ pertaining to a 'zero' crossflow, $u_0(\eta) \approx 0$. Notice that, when $K \neq 0$, $u_0(\eta)$ has, over a portion of the range of values of β shown, a reversed profile associated with the main upper solution branch for $K > 0$ (figure 7*a*) and with the lower branch when $K < 0$ (figure 7*c*). Turning now to the

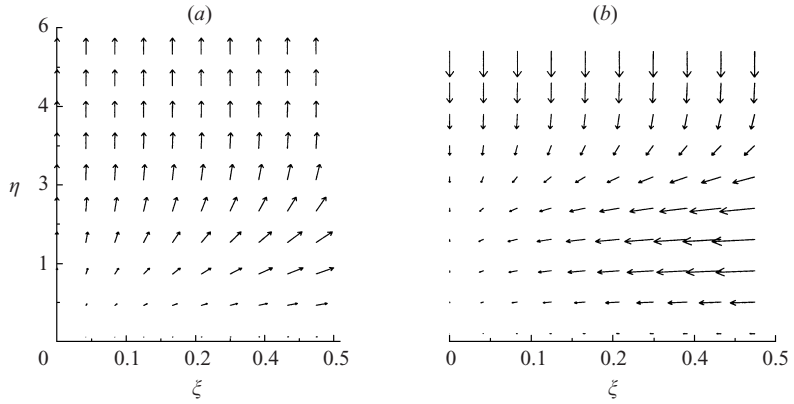

FIGURE 8. Almost planar corners, region (i), $K = 0$: secondary flow vector plots. (*a*) $\beta = 0$. (*b*) $\beta = 1.0$.

'overshoot' solution branch, we see that $u_0(\eta)$ has either a reversed profile (dotted lines) or changes its direction twice (solid lines), over a portion of the range of values of β shown in figure 6*d*; this is coupled to a marked overshoot (approaching a 'jet-like' behaviour) in the streamwise velocity solution profile $w_0(\eta)$, which suggests a substantial transfer of momentum from the secondary flow to the main flow.

To gain a deeper insight into results presented so far, a selection of vector plots of the secondary flow velocity for $K = 0$ are shown in figure 8, and over a range of (K, β) values in figure 9; in the latter figure, lower solution branch results are depicted on the left-hand side while those of the upper branch are plotted on the right-hand side. We see that the upper three-dimensional solution branch for $K = 0$ (figure 8), is associated to a secondary flow drifting upwards and away from the plane of symmetry when $\beta = 0$, but downwards and towards the said plane for $\beta = 1$. These results appear to be consistent with those of Dhanak & Duck (1997) (lower solution branch in their convention) for the rectangular corner flow. Vector plots, for the upper solution branches $K = 4$ flow state, are seen to reflect a similar behaviour. In contrast, for $K < 0$ (over the range of (K, β) shown) the secondary flow (corresponding to upper solution branches) drifts, for $\beta = 0.1$, away from the symmetry plane and upwards towards the outer reaches of the shear layer, but downwards and away from the plane of symmetry for $\beta \geqslant 0.5$. On the other hand, lower solution branches are seen to lead generally to more complex crossflow patterns characterized, for some flow states, by collisions of wall layers in the vicinity of the symmetry plane.

5.2.3. *The* $|K| \ll 1$ *case*

As pointed out above, one of the solutions obtained when $K = 0$ is the two-dimensional classical Falkner–Skan solution. In this particular case, the three-dimensional solution behaviour can be sought by solving for the perturbation solution (u_1, v_1, w_1):

$$(u_0, v_0, w_0)(\eta) = (u_{00}, v_{00}, w_{00})(\eta) + K(u_1, v_1, w_1)(\eta) + O(K^2), \tag{5.27}$$

obtained for $K \ll 1$, and satisfying $u_1(\eta = 0) = w_1(\eta = 0) = 0$ together with $u_1(\eta = \infty) = -\beta/\pi$, $w_1(\eta = \infty) = 0$, (v_{00}, w_{00}) being the Falkner–Skan solution. Again, for brevity and owing to lack of space, the corresponding equations are not given here.

Results for $w_{1\eta}(\eta = 0)$ and $u_{1\eta}(\eta = 0)$ are shown in figures 10(*a*) and 10(*b*). We see from figure 10(*a*) that both $w_{1\eta}(\eta = 0)$ and $u_{1\eta}(\eta = 0)$ exhibit a singular

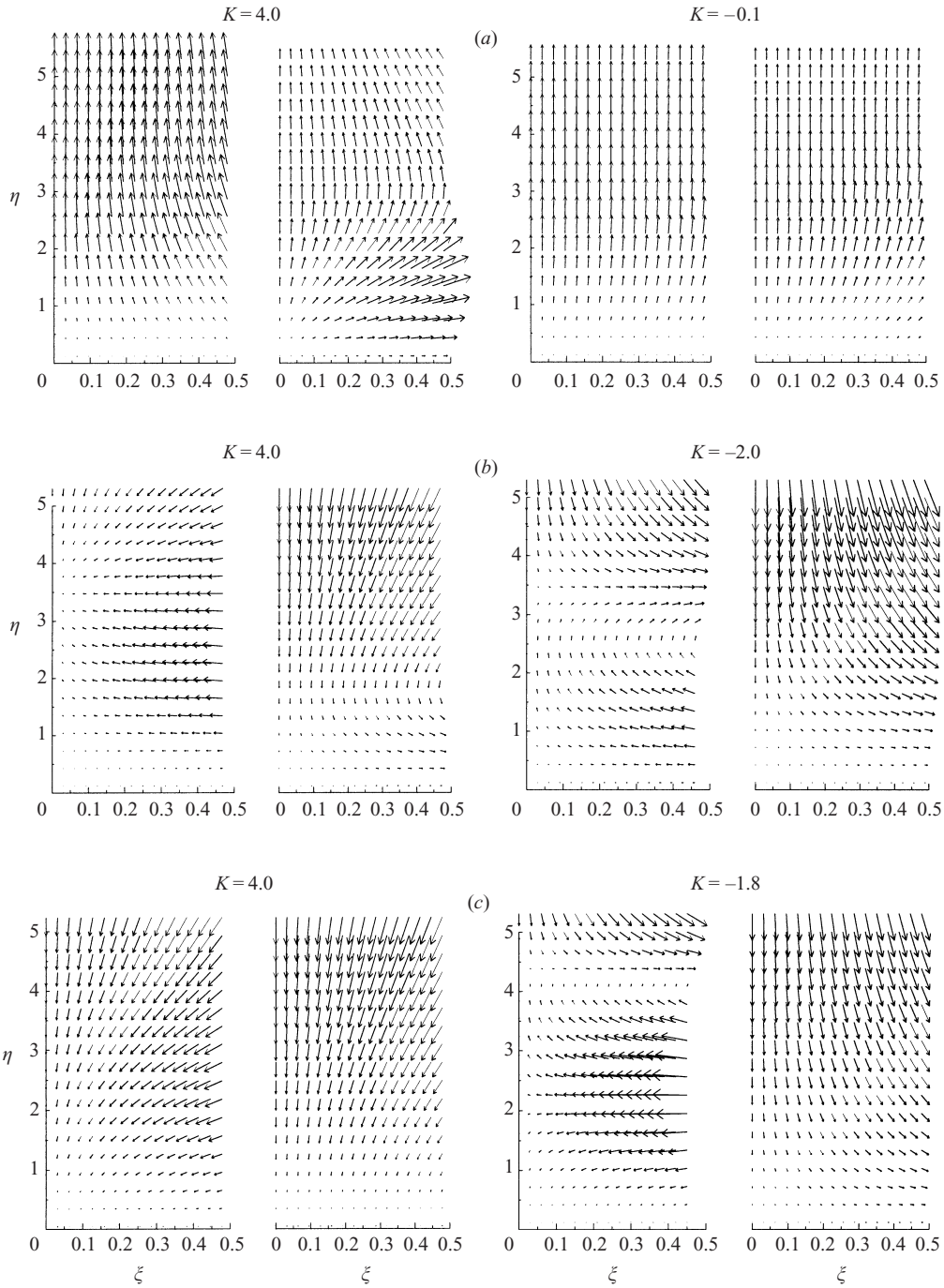

FIGURE 9. Almost planar corners, region (i), $K \sim O(1)$: secondary flow vector plots, (β, K) values as indicated. For each K value the left-hand side plot corresponds to the lower solution branch and the right-hand side to the upper branch. (*a*) $\beta = 0.1$. (*b*) $\beta = 0.5$. (*c*) $\beta = 1.0$.

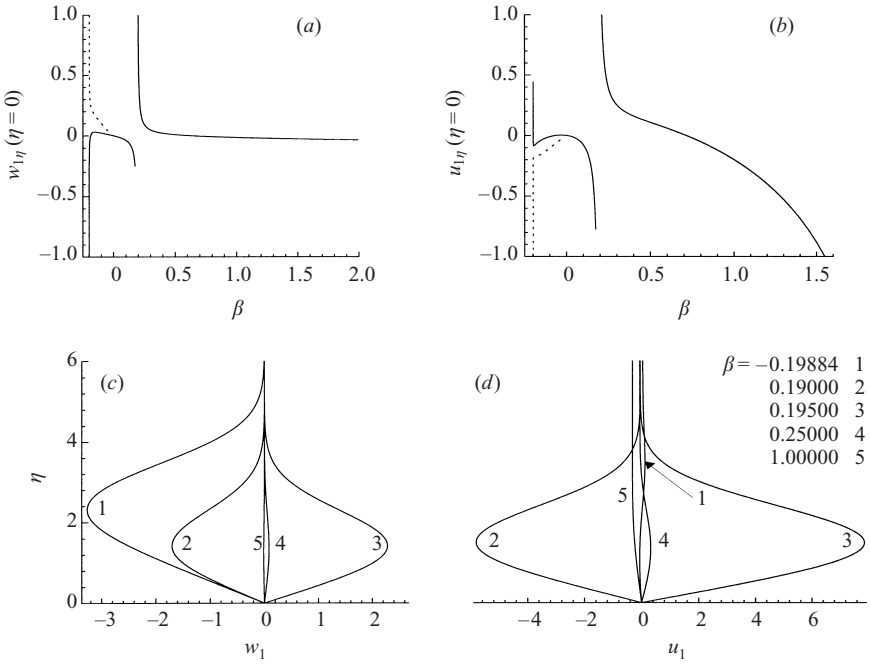

FIGURE 10. Almost planar corners, region (i), $K \ll 1$: Falkner–Skan solution branch. (*a*) $w_{1\eta}(\eta=0)$ and (*b*) $u_{1\eta}(\eta=0)$ distributions with varying β. (*c*) $w_1(\eta)$ and (*d*) $u_1(\eta)$ profiles, β as indicated.

behaviour in the vicinity of $\beta \simeq 0.193$ and at the lower bound $\beta = -0.19884$, which reflects a change in the direction of the crossflow velocity component as observed from figure 10(*d*). Comparison with solutions obtained for $K = O(1)$ reveals that the perturbation solution is consistent with those of lower solution branches for $\beta < 0.193$ and with upper ones otherwise; its behaviour near $\beta = 0.193$ is therefore a reflection of that arising close to 0.1927, at which the crossflow changes direction.

5.2.4. *The $K \to -\infty$ case*

As observed by Smith (1975) for the stagnation point flow into a corner, when K becomes large and negative, the viscous layer becomes thinner and thinner until η becomes small and $O(\exp(K/\pi))$. This is also valid here and so setting $\eta = (2\mathrm{sgn}(\beta)/\beta)^{1/2}\exp(K/\pi)\zeta$, with

$$\left.\begin{aligned} F_0 &= \tfrac{1}{2}\beta\,\mathrm{sgn}(\beta)\exp(-2K/\pi)\mathscr{F}(\zeta) + O(\exp(-K/\pi)),\\ G_0 &= \tfrac{1}{2}(2\beta\,\mathrm{sgn}(\beta))^{1/2}\exp(-K/\pi)\mathscr{G}(\zeta) + O(1),\\ H_0 &= \mathscr{H}(\zeta) + O(\exp(K/\pi)), \end{aligned}\right\} \tag{5.28}$$

we find after substitution in (5.20)–(5.23) and (5.24)

$$\frac{\mathrm{d}^3\mathscr{G}}{\mathrm{d}\zeta^3} + \mathscr{G}\frac{\mathrm{d}^2\mathscr{G}}{\mathrm{d}\zeta^2} + 1 - \left(\frac{\mathrm{d}\mathscr{G}}{\mathrm{d}\zeta}\right)^2 = 0, \quad \mathscr{F} = -\frac{\mathrm{d}\mathscr{G}}{\mathrm{d}\zeta}, \quad \frac{\mathrm{d}^2\mathscr{H}}{\mathrm{d}\zeta^2} + \mathscr{G}\frac{\mathrm{d}\mathscr{H}}{\mathrm{d}\zeta} = 0, \tag{5.29}$$

subject to $\mathscr{F}(0) = \mathscr{G}(0) = \mathrm{d}\mathscr{G}(0)/\mathrm{d}\zeta = \mathscr{H}(0) = 0$ together with $\mathscr{F}(\infty) = -\mathrm{sgn}(\beta)$, $\mathrm{d}\mathscr{G}(\infty)/\mathrm{d}\zeta = \mathrm{sgn}(\beta)$, $\mathscr{H}(\infty) = 1$. Notice that, when $\beta = 1$, equations (5.29) are essentially the same as those found by Smith (1975). Notice also that the governing equation of $\mathscr{G}$, together with the corresponding boundary conditions, reproduces the

two-dimensional stagnation point flow solution when $\beta > 0$. However, in view of the requirement of absence of exponential growth for $\mathscr{G}(\zeta)$ as $\zeta \to \infty$, there exists no solution for this equation when $\beta < 0$. Crucially, equations (5.29) suggest that, for a convex corner, the fluid motion becomes mainly determined by the secondary flow in the (x^*, y^*)-plane, a flow property which turns out also to be valid for the full problem treated in § 7.

Further, we find

$$\left.\begin{aligned} F_{0\zeta}(\zeta = 0) &= -1.23259(\beta/2)^{3/2}\exp(-3K/\pi), \\ H_{0\zeta}(\zeta = 0) &= 0.57047(\beta/2)^{1/2}\exp(-K/\pi), \end{aligned}\right\} \tag{5.30}$$

to the first order in K, which tells us that the wall shear stress is now considerably larger than for concave corner situations, $K > 0$. Such marked differences exist between the behaviour of the local flow in the two corner configurations because of the role played by the terms in (x/r_0) and $(r/r_0)^{s-1}$ in (2.25). It is clearly seen here that for concave corners ($s > 2$) the former term dominates, whereas for convex corners ($1 < s < 2$) it is the latter which becomes dominant.

6. Boundary layer in concave corners, $s > 2$

Here, attention will be focused exclusively on viscous motion in the intermediate layer. Flow in the corner layer is not considered here since it has already been treated elsewhere; for this layer, equations (5.8)–(5.11) together with appropriate boundary conditions admit similarity solutions as shown in Ridha (1990) and in Dhanak & Duck (1997), with numerical solutions and detailed discussions given in the latter. See also the work of Duck *et al.* (1999) on non-similarity solutions, in which they have considered the effects of wall transpiration.

6.1. *The intermediate layer: region* (iii)

6.1.1. *Governing equations*

In this region, we have $\delta_x = \varepsilon_x = \delta$ together with $\varepsilon_y = \delta_y = Re^{-1/2}$ by virtue of boundary-layer approximations. We find

$$\hat{U}\hat{U}_X + \hat{V}\hat{U}_Y + \hat{W}\hat{U}_z = -\delta^{-2}\hat{P}_X + \hat{U}_{YY}, \tag{6.1}$$

$$\hat{P}_Y = O(Re^{-1}), \tag{6.2}$$

$$\hat{U}\hat{W}_X + \hat{V}\hat{W}_Y + \hat{W}\hat{W}_z = -\hat{P}_z + \hat{W}_{YY}, \tag{6.3}$$

$$\hat{U}_X + \hat{V}_Y + \hat{W}_z = 0. \tag{6.4}$$

To obtain similarity solutions, we introduce the following quantities

$$\hat{U} = -z^{(m-1)/2}c^{-2}[\overline{F}(\xi,\eta) + (\beta - 1)\xi\overline{H}(\xi,\eta)], \tag{6.5}$$

$$\hat{V} = -z^{(m-1)/2}c^{-1}[\overline{G}(\xi,\eta) + (\beta - 1)\eta\overline{H}(\xi,\eta)], \tag{6.6}$$

$$\hat{W} = z^m\overline{H}(\xi,\eta), \quad \hat{P} = -\tfrac{1}{2}z^{2m} + \delta^2 z^{m-1}\overline{P}(\xi) + \cdots \tag{6.7}$$

into the boundary-layer equations, leading to

$$F_{\eta\eta} + FF_\xi + GF_\eta + (\beta - 1)\xi H^2 = Q, \tag{6.8}$$

$$H_{\eta\eta} + FH_\xi + GH_\eta + \beta(1 - H^2) = 0, \tag{6.9}$$

$$F_\xi + G_\eta - (2 - \beta)H = 0, \tag{6.10}$$

after dropping the overbar. Here,

$$Q = \tfrac{1}{4}\beta^2\xi - \frac{s\beta(2-\beta)}{4(s-1)}\xi^{s-1} + \frac{\beta^2}{4(s-1)}\xi^{2s-3},$$

on account of potential flow constraints at $\eta = \infty$.

The boundary conditions are

$$F = G = H = 0 \quad \text{at } \eta = 0, \tag{6.11}$$

together with

$$F \to \tfrac{1}{2}\xi\left[2 - \beta - \frac{\beta}{(s-1)}\xi^{s-2}\right],\ H \to 1 \quad \text{as } \eta \to \infty \tag{6.12}$$

for $\xi \in [0,1]$, in addition to a given solution at some ξ-plane. To this end, use can be made of the solution at the inner limit of region (ii) or of asymptotic solutions of system (6.8)–(6.12) for $\xi \ll 1$. This enables us, in general, to use standard marching numerical schemes from either limit depending on the sign of F appearing in the second term of equations (6.8) and (6.9). However, our efforts to solve these equations numerically by such schemes have encountered many difficulties related to the solution behaviour, particularly in the inner limit. That is why we find it preferable to discuss these issues first.

6.1.2. *Numerics and solution properties as* $\xi \to 0$ *and* $\xi \to 1$

The solution of (6.8)–(6.12) at $\xi = 1$ is readily derivable from that of system (4.6)–(4.8) and always yields $F > 0$. This suggests that a parabolic marching numerical scheme in the decreasing ξ-direction is plausible for the full problem.

On the other hand, for $\xi < 1$, with η fixed, we set

$$(F, G, H)(\xi, \eta) = \sum_{k=0}^{\infty} \xi^{k(s-2)}\,(\xi F_k, G_k, H_k)\,(\eta), \tag{6.13}$$

which can be used either as an initial boundary condition in a parabolic marching scheme or for the purpose of verification. Inserting these expansions into (6.8)–(6.10) leads, for the zeroth-order solution in ξ, to the same set of equations as (5.25), (5.20) and (5.22), respectively, with $Q_0 = \frac{1}{4}\beta^2$. The boundary conditions become

$$F_k = G_k = H_k = 0 \quad \text{at } \eta = 0, \quad \text{for} \quad k = 0, 1, \ldots, \tag{6.14}$$

together with

$$\left.\begin{aligned} &F_0 \to \tfrac{1}{2}(2-\beta), \qquad H_0 \to 1, \\ &F_1 \to -\frac{\beta}{2(s-1)},\ F_{k+1} \to 0, \quad H_k \to 0 \quad \text{for} \quad k = 1, 2, \ldots \end{aligned}\right\} \tag{6.15}$$

as $\eta \to \infty$. Note that the zeroth-order system (or its equivalent) was discussed in some detail in (Ridha 1992) and in (Dhanak & Duck 1997), and found to have a dual solution in the range $-0.0367\cdots \lesssim \beta \leqslant 2$. For reference and completeness, the distribution of $F_{0\eta}(\eta = 0)$ and $H_{0\eta}(\eta = 0)$ are shown in figure 11. Note that, here again, we will refer to that family of solutions with the greatest value of $H_{0\eta}(\eta = 0)$ as the upper solution branch, the Blasius solution belonging consequently now to the lower branch.

According to expansion (6.13), it is generally found that $F > 0$ for $\xi \ll 1$, implying that a parabolic marching numerical scheme in the positive ξ-direction is ill-posed

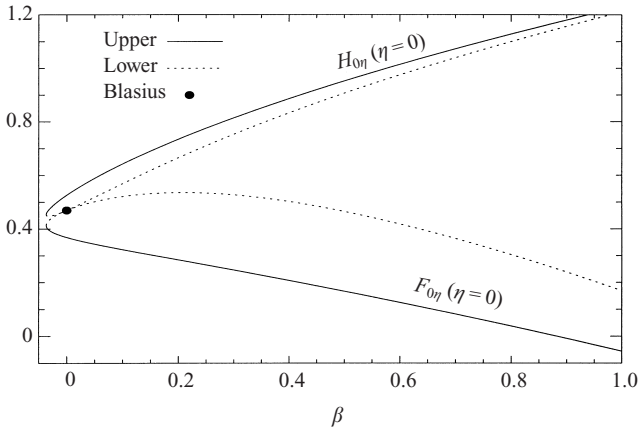

FIGURE 11. Distributions of $F_{0\eta}(\eta = 0)$ and $H_{0\eta}(\eta = 0)$ with varying β.

and must consequently be excluded. In conformity with these indications, we have implemented a fully implicit second-order finite-difference marching numerical scheme (MNS) using a Crank–Nicholson approximation in the ξ-direction with a Newton–Raphson procedure for the nonlinear terms. The resulting discrete equations are kept coupled and simultaneously solved for the vector function (F, G, H) at each ξ-plane, with initial conditions applied at $\xi = 1$. This has led to a highly convergent scheme where three to five iterations suffice to obtain a convergent solution to order 10^{-8}. It was found that: (i) converged numerical solutions reproduced always the asymptotic upper solution branch as $\xi \to 0$, and (ii) as β increased beyond a certain bound (depending on the corner angle) the numerical scheme broke down at some small value of ξ; for instance, for a 45° corner such a breakdown was found to take place at $\xi \lesssim 0.475$ when $\beta = 0.9$, whilst for a rectangular corner it occurred close to $\xi \lesssim 0.34$ when $\beta = 1.0$.

In an attempt to explain the solution behaviour as $\xi \to 0$ and the said breakdown, we assume that the basic state solution (denoted by subscript b) has eigensolutions:

$$(F, G, H)(\xi, \eta) = (\xi F_b(\eta), G_b(\eta), H_b(\eta)) + \xi^{\lambda}(\xi F_{\lambda}(\eta), G_{\lambda}(\eta), H_{\lambda}(\eta)) + \cdots . \tag{6.16}$$

These are similar to those employed in Libby & Fox (1963), Luchini (1996), Duck *et al.* (1999, 2000) and Duck & Dry (2001), but are specifically applied in the spanwise direction, and, as such, are effectively (in the final analysis) analogous to those used by Luchini (1996).† However, whereas there they were used to study algebraic growth of Reynolds-number-independent eigenmodes with respect to the streamwise distance, they are employed here to investigate algebraic growth in the spanwise direction only. One more important difference is that in Luchini (1996) it was necessary to assume spanwise disturbances of large wavelength compared with the boundary-layer thickness. Here, this is no longer so, namely because both the spanwise velocity and length scales are now of an order of magnitude (in the event, δ) greater than the normal scale $Re^{-1/2}$. Inserting expansions (6.16) into equations (6.8)–(6.10) leads to perturbation equations subject to the following boundary conditions

$$F_{\lambda}(0) = G_{\lambda}(0) = H_{\lambda}(0) = F_{\lambda}(\infty) = H_{\lambda}(\infty) = 0. \tag{6.17}$$

In view of expansions (6.13), we have taken $F_b = F_0$, $G_b = G_0$, $H_b = H_0$ which yields an eigenvalue problem independent of the corner angle, and is therefore generic in

† The author is indebted to one of the referees who brought this aspect to his attention.

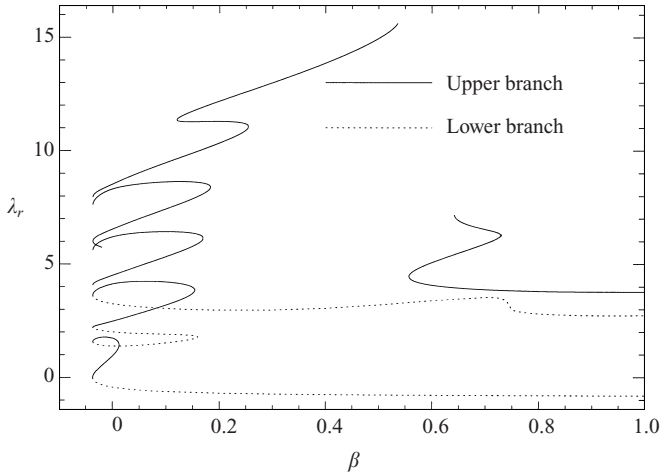

FIGURE 12. Evolution of eigenvalues with β for $s > 2$.

nature. To solve the perturbation equations, a numerical scheme, based on a fourth-order Runge–Kutta method, was used and real parts of the eigenvalue $\lambda_r = \mathrm{Re}\{\lambda\}$ are plotted in figure 12. Here, are depicted only the first few modes (the smallest in magnitude) with solutions corresponding to the primary upper solution branch sketched in solid lines and those due to the lower branch in dotted lines; note that all the shown modes are real, but complex modes have also been found. Over the range of values of β shown, the following picture has emerged: (i) for the first mode, λ_r approaches zero at the lower bound $\beta = -0.0367\ldots$ which connects the upper and lower solution branches; (ii) $\lambda_r > 0$ for the upper branch except for a number of isolated points for which $\lambda_r < 0$ (sometimes very large); and (iii) $-1 < \lambda_r \leqslant 0$ for the first mode associated with the lower solution branch. Clearly, the latter result suggests that the lower branch full-problem-solution state becomes unstable as $\xi \to 0$. That is possibly why numerical solutions obtained so far do always reproduce the upper solution branch in this limit. At this stage, we note that these results are consistent, in general, with those of Ridha (1992) (and in some sense with the recently published work of Duck & Dry (2001) on three-dimensional disturbances to boundary-layer flows) regarding the stability of solutions/flows related to (F_0, G_0, H_0). In particular, they also suggest (when projected in the physical space) that, for the lower solution branch (and should the corresponding flows exist in nature), the u-component of the perturbation would be expected to decay in the intermediate layer (if the pressure gradient is not too small), but its w-component would grow unboundedly as $x \to 0$. This regime is analogous to the spatial instability mechanism discussed by Luchini (1996) in his study of the Blasius boundary-layer instability, which he proposed as a good candidate for the initial linear-amplification stage of bypass transition. Importantly, when coupled to the recent investigation of Parker & Balachandar (1999) on viscous and inviscid instabilities of a flow along a streamwise corner, in which they have found that the growth rate of incoming oblique disturbances is enhanced by the corner (compared to a decreasing growth rate of outgoing disturbances), these results raise the issue of the flow instability in the inner limit of the intermediate layer, and of its role in the overall (or its effect on the corner) boundary-layer instability.

In view of the above, and in order to overcome the breakdown problem, we have treated system (6.8)–(6.10) as a pseudo-elliptic for which boundary conditions at

$\xi = 1$ and at some small value of ξ were applied, and used a Newton–Raphson iterative direct numerical scheme (DNS) to solve for all grid points simultaneously. This enabled us to overcome the breakdown problem encountered by the parabolic marching scheme (MNS) in so far as the upper branch is concerned, but difficulties faced in the computations of the lower branch solutions persisted. Many numerical experimentations were conducted with lower branch boundary conditions (obtained using four-term solutions based on expansions (6.13)) imposed at $\xi = \xi_0 \leqslant 0.1$ for various values of β. It was found that solutions obtained for $\beta > 0.5$ coincided for most of the computational domain with the upper branch solutions, and suffered from marked oscillations as ξ_0 is approached; these were observed to spread out throughout the computational domain for $\beta \lesssim 0.5$. Such a behaviour strongly hints that the occurrence of eigensolutions associated with the lower branch seems to be the principal source behind our computational difficulties. Finally, a further attempt to overcome this problem imposed itself, namely using TVD (total variation diminishing) schemes in which artificial dissipation can be introduced (in a controlled nonlinear fashion) in order to damp out the effect of the eigensolutions. To this end, we have implemented various procedures based on schemes suggested by Davis (1984), Yee (1987) and more recently by Sun & Takayama (1999) for the two-dimensional Euler equation. Our choice was mainly conditioned by the fact that system (6.8)–(6.10), when written in conservative form, leads to Jacobian matrices (arising in TVD methods) which are singular. Throughout, the computational difficulties associated with the lower branch solution persisted and it became obvious that this problem goes beyond the scope of the present paper.

6.1.3. *Results and further discussion*

Numerous computations were conducted for corners of angles $\pi - 2\alpha = 45^\circ$, 90° and 135°, the results of which suggested that it suffices to focus attention on the rectangular corner situation. Results for this case are presented in figures 13–15 in terms of $u(\xi, \eta)$ and $w(\xi, \eta)$ for the velocity variables, and $\omega(\xi, \eta) = -u_\eta/c$ for the streamwise vorticity.

For the upper solution branch, we start by focusing our attention on distributions of $w_\eta(\xi, \eta = 0)/c$ and $u_\eta(\xi, \eta = 0)/c$, shown in figure 13 for various values of β, while at the same time recalling that the skin friction vanishes at the corner line (Zamir & Young 1970; Rubin & Grossman 1971; Barclay 1973; Barclay & Ridha 1980; Dhanak & Duck 1997). This, when taken into account, enables us to observe a striking qualitative resemblance between our theoretical results for $w_\eta(\xi, \eta = 0)$ (figure 13*a*, specifically for small values of the pressure gradient parameter β, particularly for $\beta = 0.05$), and the experimental ones of Zamir & Young (1970), corresponding to laminar flow along a rectangular corner under 'zero' streamwise pressure gradient conditions. However, we shall refrain from drawing definite conclusions from this resemblance in view of differences stemming from length scales of the corner and intermediate layers together with, which is more important, the effect of the pressure gradient coupled to the leading edge form on the flow stability, and eventually on the interpretation of the experimental results. From figure 13(*b*), we generally observe that the x-component of the wall shear stress, $u_\eta(\xi, \eta = 0)/c$, exhibits a non-monotonic behaviour qualitatively similar to that of the flat-plate limit, depicted in figure 4. Results illustrating the crossflow evolution and constant vorticity contours are shown in figure 14. These do appear to constitute a regular extension of those of the flat-plate limit, shown in figures 5(*a*) and 5(*b*), and confirm further the (conjecture-based) prediction made by Moore (1956) regarding the existence of a vortex pair originating

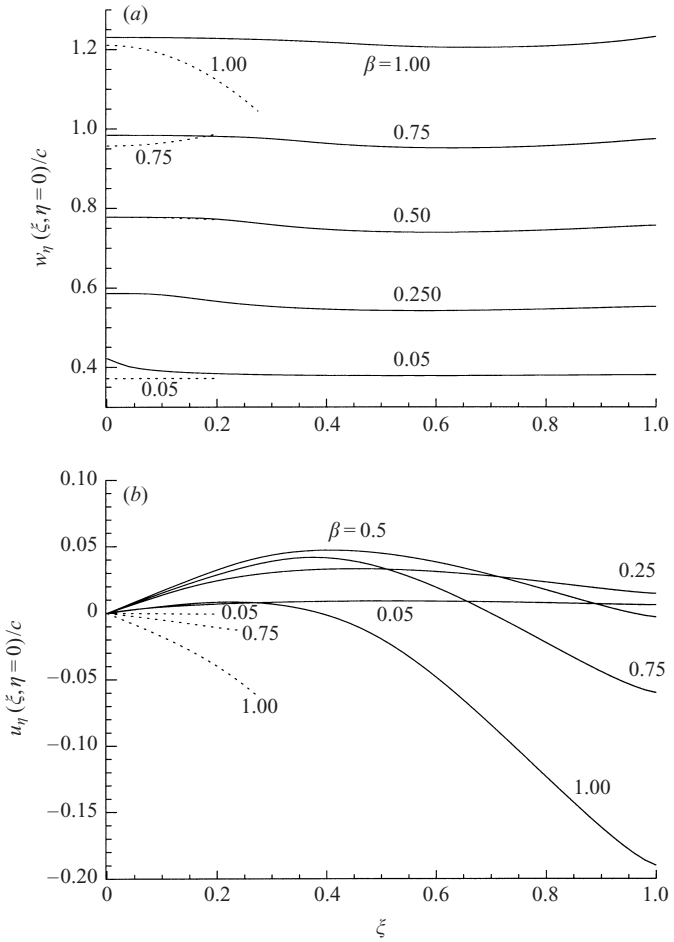

FIGURE 13. Rectangular corner configuration, region (iii): (*a*) $w_\eta(\xi,\eta=0)$ and (*b*) $u_\eta(\xi,\eta=0)$ distributions, β as indicated: $\cdots$, lower; ——, upper.

from the corner vertex. Note that, in the present flow state, a two-layer vorticity (negative in the wall vicinity and positive far from the wall) is now obtained for $0<\beta\lesssim 1$ compared to $0<\beta\lesssim 0.706\cdots$ for almost planar corners.

With regards to the lower solution branch, results are computed using a four-term approximation according to (6.13); these are shown in figure 13, plotted in dotted lines for distributions of $w_\eta(\xi,\eta=0)/c$ and $u_\eta(\xi,\eta=0)/c$, and in figure 15 for the crossflow profiles, $u(\xi,\eta)$. From the former figure, we observe that they differ considerably from those of the upper branch solution, particularly for $\beta=1$, and exhibit a non-monotonic behaviour over the range of values of β and ξ shown. Turning to the evolution of crossflow profiles, figure 15 suggests that a closed streamwise vortex would also be generated within the intermediate layer for moderately small values of β.

The overall flow picture emerging thus far raises further questions, certainly worthy of investigation, concerning corner flow instability particularly in the light of the occurrence of eigensolutions discussed in the previous subsection, and in relation to the crossflow–vortex structure. On the whole, this appears to be consistent with difficulties described by Zamir (1981) in observing stable laminar flow in a corner under conditions of zero streamwise pressure gradient at large Reynolds numbers.

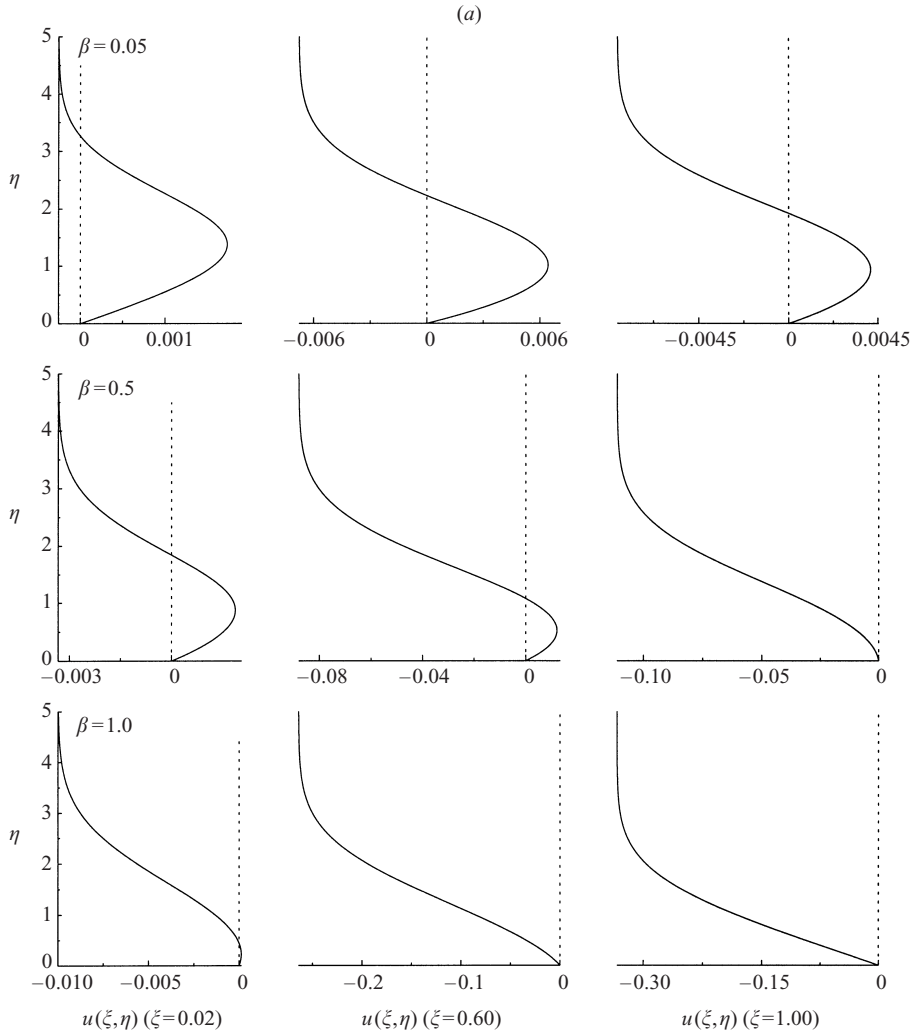

FIGURE 14(*a*). For caption see facing page.

7. Boundary-layer flow in convex corners, $1 < s < 2$

7.1. *The corner layer: region* (i)

For convex corners, the order of magnitude estimations, (3.4), show that $(\delta Re)^{-1} \leqslant \hat{\delta} \leqslant Re^{-1/2}$ with $\delta \geqslant \varepsilon \geqslant Re^{-1/2}$ over the range $1 \leqslant s \leqslant 2$. This tells us that the corner layer is much thinner than was previously reported by Barclay & Ridha (1980) for the strictly zero streamwise pressure gradient case. In that work, both $\hat{\delta}$ and ε were taken to be $O(Re^{-1/2})$.

In view of of these estimations, boundary-layer approximations lead (for s sufficiently smaller than two) to the following boundary-layer equations

$$\hat{U}\hat{U}_X + \hat{V}\hat{U}_Y = -P_X + \hat{U}_{XX} + \hat{U}_{YY}, \tag{7.1}$$

$$\hat{U}\hat{V}_X + \hat{V}\hat{V}_Y = -P_Y + \hat{V}_{XX} + \hat{V}_{YY}, \tag{7.2}$$

$$\hat{U}\hat{W}_X + \hat{V}\hat{W}_Y = \hat{W}_{XX} + \hat{W}_{YY}, \tag{7.3}$$

$$\hat{U}_X + \hat{V}_Y = 0, \tag{7.4}$$

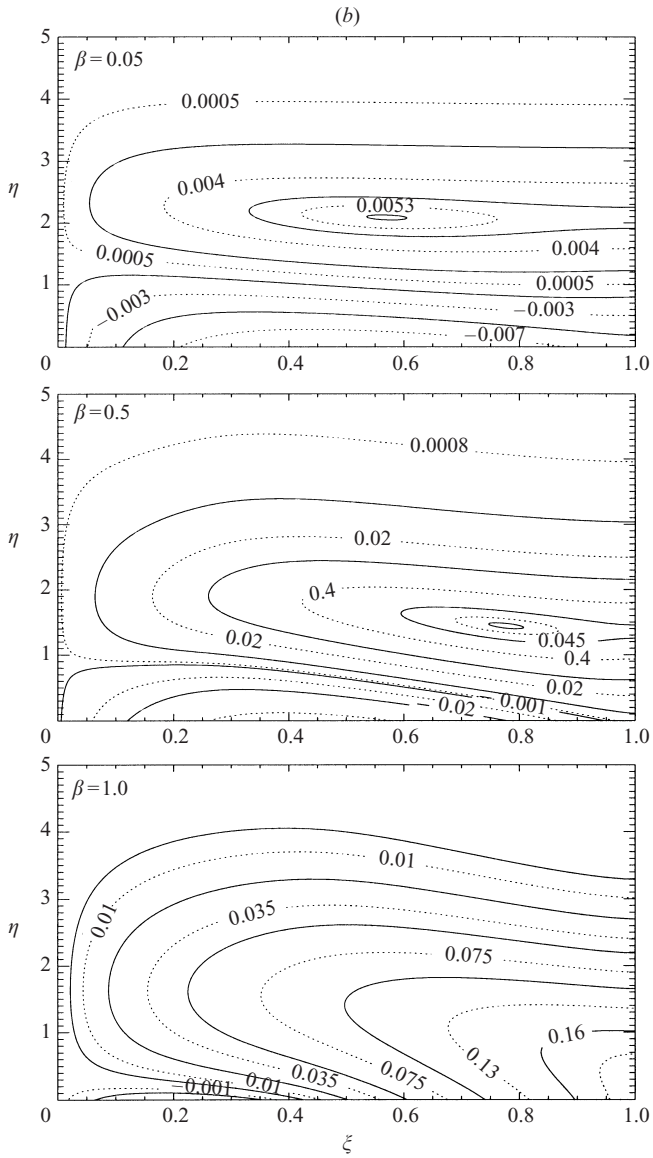

FIGURE 14. Rectangular corner configuration, upper solution branch in region (iii): (*a*) evolution of $u(\eta, \xi)$ profiles, β and ξ as indicated. (*b*) streamwise vorticity $\omega(\eta, \xi)$ contours, β as indicated.

for which we have set

$$\hat{P} = P_0(z) + (Re\hat{\delta})^{-1} P_1(X, Y, z) + (Re\hat{\delta})^{-2} P(X, Y, z) + \cdots . \tag{7.5}$$

This outcome is rather surprising, and is in striking contrast with that obtained for the concave corner situation, for system (7.1)–(7.4) contains no derivatives with respect to the streamwise direction (the z-axes), and this is despite the fact that close to the corner line the flow is expected to be fully three-dimensional. Nevertheless, such a result is not confined to this particular corner problem since an analogous situation was reported for boundary-layer motion in the neighbourhood of the intersection of a concave cylindrical surface and a plane surface (Gurevich 1981), and close to the line of intersection of curved surfaces (Gurevich 1985).

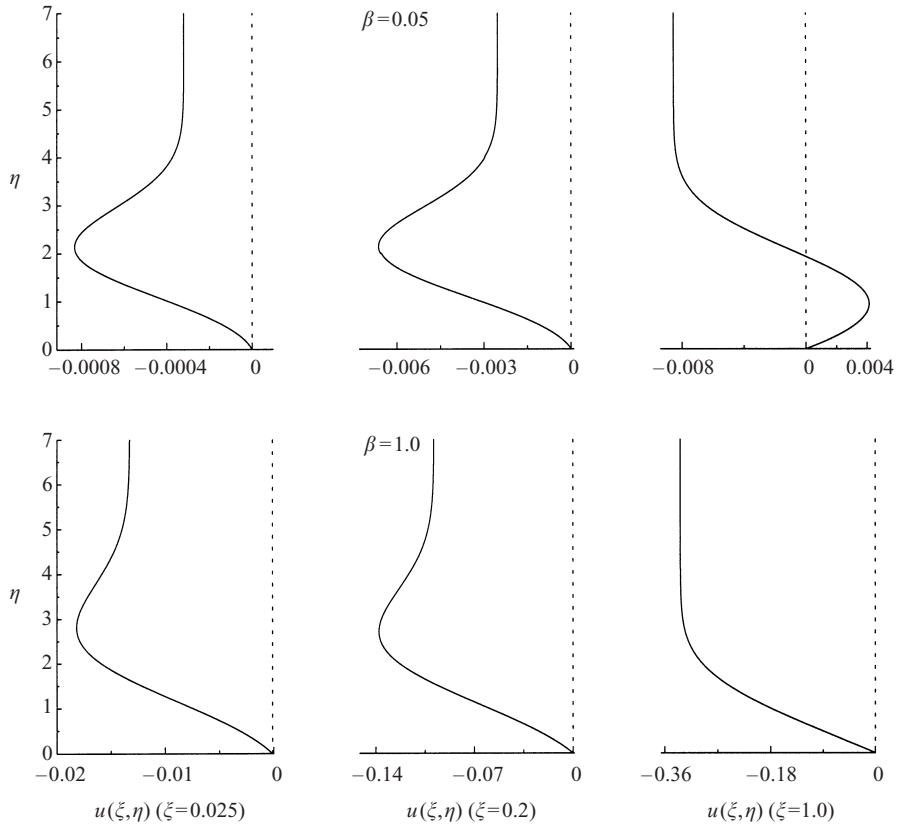

FIGURE 15. Rectangular corner configuration, lower solution branch in region (iii): $u(\eta, \xi)$ profiles, β and ξ as indicated. Profiles at $\xi = 0.025, 0.2$ are computed by using expansions (6.13).

Here, we immediately see that (7.1), (7.2) and (7.4) are effectively the two-dimensional Navier–Stokes equations. We also observe that the pressure gradient term is now absent from the streamwise momentum equation, (7.3). This is a crucial result which tells us that the viscous motion in a convex corner is determined mainly by a primarily two-dimensional (secondary) flow past a 'wedge' of opening angle $\tilde{\alpha} = (2-n)\pi$ (compared to $\beta\pi$ for the classical two-dimensional wedge), where $n = 2/s$ with $1 \leqslant n \leqslant 2$. It follows, therefore, that as $n \to 1$ (i.e. in the semi-infinite flat plate limit) the flow in the (x^*, y^*)-plane becomes effectively that of a two-dimensional stagnation point flow which confirms results presented in § 5.2.4 for $K \to -\infty$. Furthermore, equations (7.1), (7.2) and (7.4) indicate that in the quarter-infinite flat-plate limit $n \to 2$, the fluid motion in the (x^*, y^*)-plane would correspond to that past a semi-infinite flat plate at zero incident. In particular, it can be shown that as $X \to \infty$, with $Y \sim 1$ fixed, the crossflow corner-layer solution assumes a Falkner–Skan-like form, but with a solution existing only for $\beta > 0$ for reasons similar to those given in § 5.2.4, namely because of the governing equations admitting exponentially decaying solutions as $Y \to \infty$ only when $\beta > 0$.

The above result further suggests that, for convex corners, the Stokes solution of the secondary flow problem is none other than that found by Moffat (1964), and by Davis, Ghia & Ghia (1974) whose results additionally provide, apart from a multiplication factor, practically the full corner-layer secondary flow solution.

7.2. *The intermediate layer: region* (iii)

7.2.1. *Governing equations*

In this region, equations (6.1)–(6.4), and the corresponding similarity equations (6.8)–(6.10), remain valid, of course; but as $\xi \to 0$, conditions imposed on $F(0,\infty)$ and $G_\eta(0,\infty)$ become unbounded. To take this behaviour into account, we seek then similarity-type solutions by introducing the following new variables

$$\left.\begin{aligned} \hat{U} &= -\mathscr{Z}[\overline{\mathscr{F}}(\xi_1,\eta_1) + \tfrac{1}{2}s(\beta-1)J_1\xi_1\overline{\mathscr{H}}(\xi_1,\eta_1)],\\ \hat{V} &= -\mathscr{Z}[(n-1)\eta_1\overline{\mathscr{F}}(\xi_1,\eta_1) + \xi_1\overline{\mathscr{G}}(\xi_1,\eta_1) + (\beta-1)J_1\xi_1\eta_1\overline{\mathscr{H}}(\xi_1,\eta_1)],\\ \hat{W} &= z^m\overline{\mathscr{H}}(\xi_1,\eta_1),\ \hat{P} = -\tfrac{1}{2}z^{2m} + \delta^2 z^{m-1}\overline{P}(\xi_1) + \cdots \end{aligned}\right\} \tag{7.6}$$

where $\mathscr{Z} = z^{(m-1)/2}c^{-2}J_1^{-1/2}$, $X = z^{(1-m)/2}\xi_1^n$, $Y = z^{(1-m)/2}cJ_1^{1/2}\eta_1$, $J_1 = n^2\xi_1^{2(n-1)}$, and $n = 2/s$. Inserting these into the boundary-layer equations (6.1)–(6.4) yields

$$\frac{\partial^2\mathscr{F}}{\partial\eta_1{}^2} + \mathscr{F}\frac{\partial\mathscr{F}}{\partial\xi_1} + \mathscr{G}\frac{\partial\mathscr{F}}{\partial\eta_1} - \frac{n-1}{\xi_1}\mathscr{F}^2 + \tfrac{1}{2}s(\beta-1)\xi_1 J_1^2\mathscr{H}^2 = \mathscr{Q}, \tag{7.7}$$

$$\frac{\partial^2\mathscr{H}}{\partial\eta_1{}^2} + \mathscr{F}\frac{\partial\mathscr{H}}{\partial\xi_1} + \mathscr{G}\frac{\partial\mathscr{H}}{\partial\eta_1} + \beta J_1(1-\mathscr{H}^2) = 0, \tag{7.8}$$

$$\frac{\partial\mathscr{F}}{\partial\xi_1} + \frac{\partial\mathscr{G}}{\partial\eta_1} - (2-\beta)J_1\mathscr{H} = 0, \tag{7.9}$$

after dropping the overbar; here,

$$\mathscr{Q} = \frac{2\beta^2}{s^3(s-1)}\xi_1 - \frac{\beta(2-\beta)}{2(s-1)}\xi_1 J_1 + \tfrac{1}{8}s\beta^2\xi_1 J_1^2.$$

The boundary conditions are

$$\left.\begin{aligned} &\mathscr{F} = \mathscr{G} = \mathscr{H} = 0 \quad \text{at } \eta_1 = 0,\\ &\mathscr{F} \to \xi_1\left(\tfrac{1}{4}s(2-\beta)J_1 - \frac{\beta}{s(s-1)}\right), \quad \mathscr{H} \to 1 \quad \text{as } \eta_1 \to \infty \end{aligned}\right\} \tag{7.10}$$

together with an initial condition at some $0 \leqslant \xi_1 \leqslant 1$ value by virtue of the parabolic nature of system (7.7)–(7.9), or with conditions applied at both limits as for (6.8)–(6.10). This depends on the sign of $\mathscr{F}$ appearing in the second term of the first two equations and linked, in many respects, to the nature of the solution near $\xi_1 = 0$ and $\xi_1 = 1$. That is why we find it preferable to discuss these issues first in some detail.

7.2.2. *Numerics and solution properties as* $\xi_1 \to 0$ *and* $\xi_1 \to 1$

The solution behaviour as $\xi_1 \to 0$ can be deduced by setting

$$(\mathscr{F},\mathscr{G},\mathscr{H})(\xi_1,\eta_1) = \sum_{k=0}^{\infty} J_1^k(\xi_1\mathscr{F}_k, \mathscr{G}_k, \mathscr{H}_k)(\eta_1), \tag{7.11}$$

subject to conditions readily derivable from (7.10). Inserting expansions (7.11) into equations (7.7)–(7.9) leads to sets of equations in the leading order of which the solution $(\mathscr{F}_0,\mathscr{G}_0)$ is uncoupled from $\mathscr{H}_0$, with the latter depending on the former. We find, in particular, that $(\mathscr{F}_0,\mathscr{G}_0)$ reduces to the Falkner–Skan solution $f(\eta)$ (equation (5.4)) upon writing

$$\mathscr{F}_0(\eta_1) = -a^2 f'(\eta), \quad \mathscr{G}_0(\eta_1) = af(\eta), \quad \eta = a\eta_1, \tag{7.12}$$

with the transverse pressure gradient parameter $(2-n)$ replacing β in (5.4), where $a=\sqrt{\beta/s(s-1)}$; this shows that $\mathscr{F}<0$ for ξ_1 sufficiently small. This result tells us that matching is assured between regions (i) and (iii), and suggests further that the boundary-layer flow for ξ_1 small becomes mainly controlled by the secondary flow in the (ξ_1,η_1)-plane.

Turning now to solution properties in the neighbourhood of $\xi_1=1$, we note, according to the boundary conditions (7.10), that $\mathscr{F}(1,\infty)>0$ for $\beta<(2-n)$, in which case a change of sign of $\mathscr{F}$ would be expected to occur at some $\xi_1<1$. For $\beta<(2-n)$, this observation together with that made regarding solutions behaviour for small ξ_1, indicates that: (i) $\mathscr{F}$ is likely to have a reversed profile within the domain $0<\xi_1<1$, and (ii) a marching parabolic numerical scheme started from $\xi_1=0$ (respectively, $\xi_1=1$) will most probably fail to reach $\xi_1=1$ (respectively, $\xi_1=0$).

In line with these observations, two parabolic marching numerical schemes were implemented, both analogue to scheme MNS (discussed in §6.1.2): scheme MNS_0 with initial conditions imposed at the inner limit, and scheme MNS_1 in which they were applied at $\xi_1=1$. Using both schemes numerous computations were conducted, in particular for corners of angles 225°, 270° and 315°. Here, we find it sufficient to present results for a 270° corner, for which distributions of wall shear stress components $J^{-1/2}w_{\eta_1}(\xi_1,\eta_1=0)/c$ and $J^{-1/2}u_{\eta_1}(\xi_1,\eta_1=0)/c$ (corresponding, respectively, to $w_\eta(\xi,\eta=0)/c$ and $u_\eta(\xi,\eta=0)/c$) are shown in figure 16; notice how the streamwise component of the wall shear stress tends to infinitely large values as $\xi_1\to 0$. When $\beta\leqslant(2-n)$, we have generally found that: (i) scheme MNS_0 broke down at $\xi_1<\xi_s$, (ii) scheme MNS_1 broke down at $\xi_1>\xi_s$ with $\mathscr{F}$ exhibiting a reversed-flow-like profile, and (iii) solutions obtained using scheme MNS_0 (respectively, MNS_1) were characterized by high-frequency oscillations as $\xi_1\nearrow\xi_s$ (respectively, as $\xi_1\searrow\xi_s$), where ξ_s is defined by $\mathscr{F}_{\eta_1}(\xi_s,0)=0$. In addition to these properties, our numerical results indicate that the breakdown of scheme MNS_0 occurs in a singular fashion, with $\mathscr{F}_{\eta_1}(\xi_1,0)\propto(\xi_s-\xi_1)^{1/2}$ immediately ahead of ξ_s. This suggests that a Goldstein (1948) type singularity takes place in this vicinity, as is usually encountered in calculations of separating fully two-dimensional boundary layers with prescribed adverse (positive) pressure gradient. Under such conditions, computations in the neighbourhood of ξ_s are not possible or appropriate, and must therefore be conducted within the framework of interactive boundary-layer theory (Neiland 1969; Stewartson & Williams 1969; Sychev *et al.* 1998). This is consistent with oscillations characterizing the solutions in the neighbourhood of ξ_s, which appear to mirror the dependence of solutions on downstream conditions that remain unsatisfied by both marching schemes. Furthermore, our unsuccessful attempts to overcome these difficulties by implementing approaches, using conditions near $\xi_1=0$ and at $\xi_1=1$ simultaneously, such as DNS-type or TVD schemes (see §6.1.2), seem to confirm the existence of a Goldstein type singularity.

In an attempt to gain a deeper insight into these difficulties, we have also assumed that the sought solution may have eigensolutions in the form

$$(\mathscr{F},\mathscr{G},\mathscr{H})(\xi_1,\eta_1)=(\mathscr{F}_b(\eta_1),\mathscr{G}_b(\eta_1),\mathscr{H}_b(\eta_1))+\xi_1^{n\lambda}(\xi_1\mathscr{F}_\lambda(\eta_1),\mathscr{G}_\lambda(\eta_1),\mathscr{H}_\lambda(\eta_1))+\cdots, \tag{7.13}$$

as suggested by expansions (7.11). Here, the basic state solution is denoted by the subscript b, with λ being an arbitrary complex constant. We have found that the perturbation equations for $(\mathscr{F}_\lambda,\mathscr{G}_\lambda)$ are uncoupled from that of $\mathscr{H}_\lambda$, with the

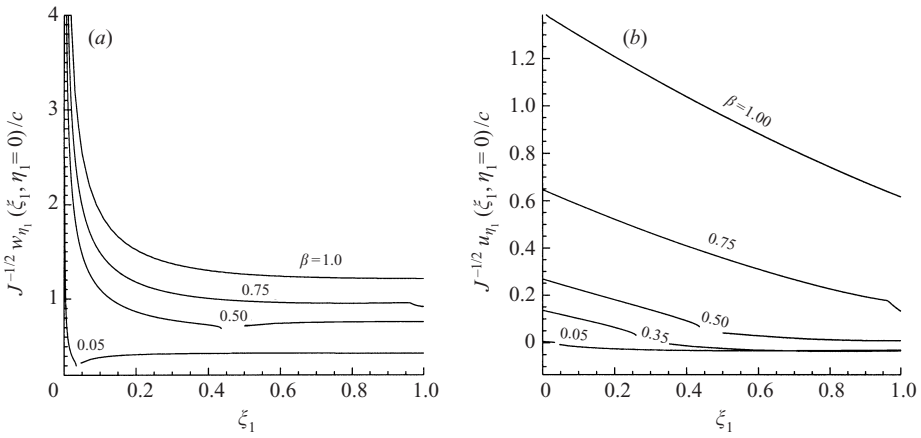

FIGURE 16. 270°-convex corner, region (iii): wall shear stress (*a*) $J^{-1/2}w_{\eta_1}(\xi_1, \eta_1 = 0)/c$ and (*b*) $J^{-1/2}u_{\eta_1}(\xi_1, \eta_1 = 0)/c$ distributions, β as indicated.

latter depending on the former; the boundary conditions are $\mathscr{F}_\lambda(0) = \mathscr{G}'_\lambda(0) = \mathscr{H}_\lambda(0) = \mathscr{F}_\lambda(\infty) = \mathscr{H}_\lambda(\infty) = 0$. For simplicity, we took $\mathscr{F}_b = \mathscr{F}_0, \mathscr{G}_b = \mathscr{G}_0$ and $\mathscr{H}_b = \mathscr{H}_0$, leading to an eigenvalue problem the numerical solution of which is independent of β, and can surprisingly be expressed (for the smallest eigenvalue) by $Re\{\lambda_1\} = 1.957\,31(1-s) - s < 0$, since $1 \leqslant s < 2$. Note that this result recovers that of Libby & Fox (1963) for the Blasius solution, presently obtained in the quarter-infinite flat plate limit $n = 2/s = 2$, and, when projected in the physical space, specifically tells us that *all* velocity components of the perturbation become unbounded as $x \to 0$. In some sense, this is consistent with the corresponding result for concave corners and sheds further light on instability problems akin to boundary-layer flows along corners and sharp edges.

7.2.3. *Results and further discussions*

Here, attention will be focused mainly on the 270° ($n = 1.5$) corner situation for which a selection of solution profiles for the crossflow velocity component $u(\xi, \eta)$ is shown in figure 17(*a*). From these results, and those depicted in figure 16(*b*) for the x-component of the wall shear stress, we see that $u(\xi, \eta)$ exhibits a reversed flow profile for values of β satisfying $\beta \lesssim (2 - n) = 0.5$ which is in line with previous discussions, and consequently mirrors the generation of a closed streamwise vortex structure as illustrated in figure 17(*b*), the vortex being rotated now in the opposite sense to that generated in concave corners. This result extends therefore the prediction made by Moore (1956) to convex corners. Another observation that deserves mention here concerns the boundary-layer thickness. This is found (when $n < 2$) to be fairly constant for β small, but becomes rapidly thinner in the inner limit of region (iii) with increasing β.

Lastly, previous discussions, together with inspection of results furnished by our numerous computations, seemingly suggest that the 'condition' $\beta \sim (2 - n)$ reflects a kind of equilibrium state between the streamwise and transverse pressure forces that manifests itself through the ratio $m/(s - 1)$ appearing in the V_x velocity component, equation (2.25), which, if m remains finite, becomes singular in the quarter-infinite flat-plate limit $n \to 2$ ($s \to 1$). This question is considered next.

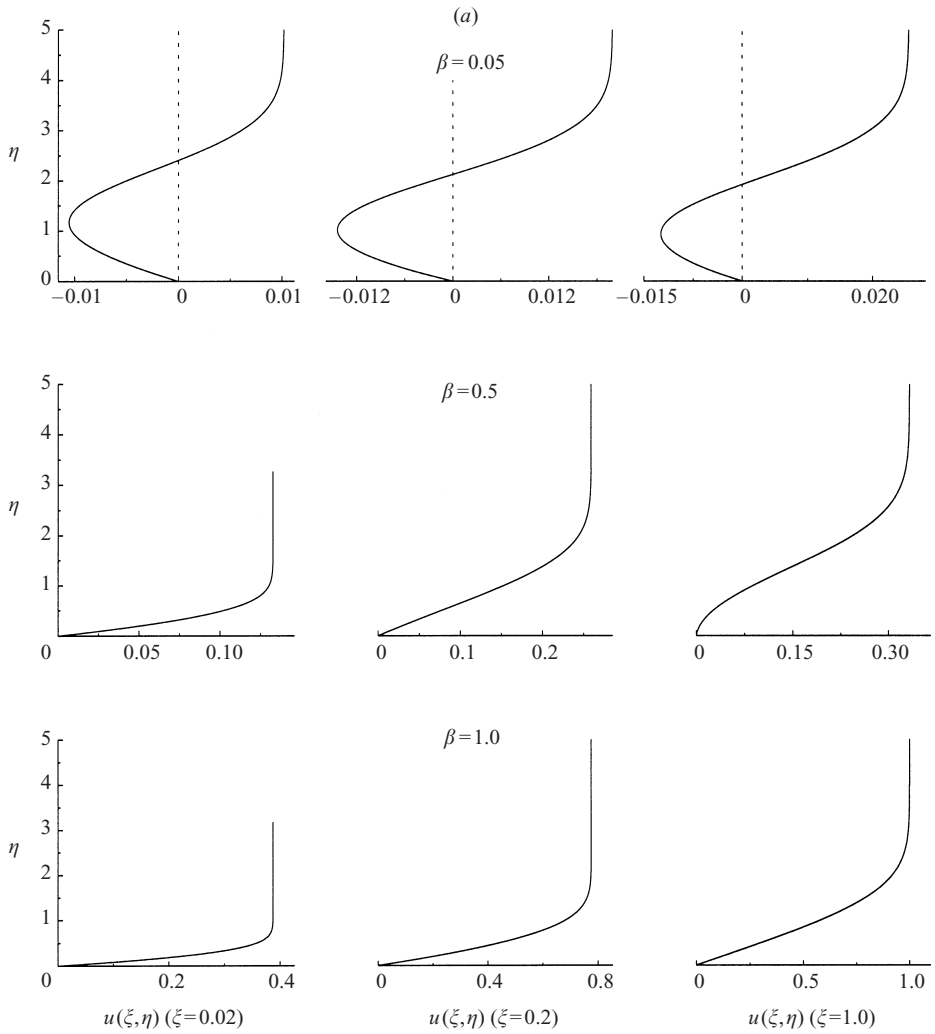

FIGURE 17(*a*). For caption see facing page.

8. The quarter-infinite flat plate limit $s \to 1$

The question of singularity arising when $s \to 1$, with $m \neq 0$, can be resolved readily, if the condition $\beta \leqslant (2-n)$ is satisfied, by letting the wedge opening angle $\alpha_w \to 0$ at this limit (implying $m \to 0$ simultaneously). Hence, we set

$$\lim_{s\to 1} m \to s-1 \to \frac{\tilde{\alpha}}{2\pi}, \quad \tilde{\alpha} \ll 1, \tag{8.1}$$

in which $\tilde{\alpha} = (2-n)\pi$ denotes the external corner angle. Note that this limiting process is exactly equivalent to setting $\lim_{n\to 2} \beta \to (2-n)$ which highlights further the physical significance of the situation previously defined by $\beta \sim (2-n)$. Now, as for an almost-planar corner, it can be shown in the present case that flow features pertaining to boundary-layer flow along a convex corner may arise when $\tilde{\alpha} = O(1/\ln(\delta/\hat{\delta}))$ or greater. However, since $\hat{\delta} \ll Re^{-1/2}$ (as $s \to 1$) we can then set $\hat{\delta} \sim Re^{-1/N}, 0 < N < 2$,

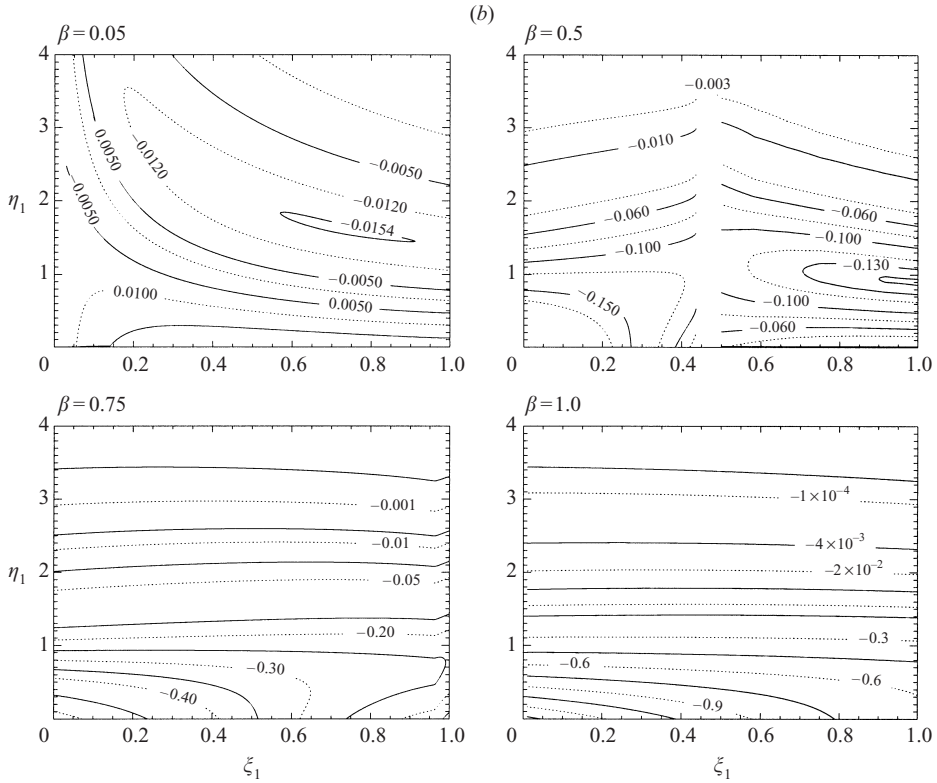

FIGURE 17. 270°-convex corner, region (iii): (*a*) $u(\xi,\eta)$ profiles, β and ξ as indicated; (*b*) constant streamwise vorticity $\omega(\xi_1,\eta_1)$ contours.

and hence we may write

$$\tilde{\alpha} = \frac{K}{\ln Re}, \quad K \sim 1 \tag{8.2}$$

before considering boundary layers in the different zones. Accordingly, the boundary-layer solution may be sought in the form

$$(\hat{U},\hat{V},\hat{W}) = (U_0,V_0,V_0) + \frac{K}{\ln Re}(U_1,V_1,W_1) + \cdots \tag{8.3}$$

where (U_0,V_0,W_0) and (U_1,V_1,W_1) are functions of (X,Y,z). In region (i) the boundary-layer equations are of course (7.1)–(7.4) where, apart from a multiplication factor, the solution (U_0,V_0) is practically that given by Davis *et al.* (1974) for the two-dimensional flow near the leading edge of a semi-infinite flat plate at zero-incidence. At the side-edge of region (i), that is for X large and $Y \sim 1$ fixed, both velocity components in the x- and z-directions can be shown to have a Blasius-type solution profile to the leading order of approximation.

For convenience, we consider now the outer boundary layer, region (ii), for which the potential flow condition imposed on the x-direction velocity component v_x leads to

$$\hat{U} \sim O(\delta\varepsilon_x^{-1}) + O(\delta\varepsilon_x^{-1}/\ln Re) \tag{8.4}$$

as $Y \to \infty$. According to Stewartson (1961), changes produced by the boundary-layer displacement effect on v_x with (x/z) small (but still sufficiently 'far' from the side-edge of the plate) are characterized by $\varepsilon_x = O(Re^{-1/2})$ and may subsequently be neglected

here compared to $O(\delta)$. Hence, we find, in conformity with problem (4.1)–(4.8), that $\hat{W} = f'(\eta)$ and

$$\hat{U} = \tfrac{1}{2} z^{-1/2} f''(\eta) \int_0^\eta \frac{\tau - \sigma}{f''(\tau)}\, \mathrm{d}\tau, \quad \sigma = \lim_{\eta \to \infty} (f - \eta), \tag{8.5}$$

to the leading order of approximations. This, apart from the order of magnitude of the x-direction velocity component, represents precisely the leading-term solution obtained by Stewartson for the viscous flow past a quarter-infinite flat plate for (x/z) small. He also finds that $\varepsilon_x = O(\ln Re/Re^{1/2})$ somewhere in a region nearer to the side-edge of the plate with (x/z) being always small, but where $\varepsilon_x = O(\delta_x)$ (in our notations). Then, in order to have a meaningful comparison with his work we set $\delta = O(\ln Re/Re^{1/2})$, and so the said region (of Stewartson) now becomes equivalent to region (iii); this estimation appears to be plausible and agrees with $1 \gg \delta \gg Re^{-1/2}$, leading to a corner layer of thickness $\hat{\delta} \sim O(1/Re^{1/2} \ln Re)$.

This brings us to the boundary layer in region (iii). Here, the governing equations are (6.1)–(6.4) for which the similarity solution can now be obtained from (7.6)–(7.10) with $m = \beta = 0$ save for $\beta/(s-1)$ which, according to (8.1) and the definition of β, is set equal to 2. Likewise, the flow properties for $\xi_1 \ll 1$ are now determined according to expansions (7.11); these provide boundary conditions at some small ξ_1. The boundary conditions at $\xi_1 = 1$, on the other hand, are furnished by g and f given in (4.6) and (4.7). These show that $\mathscr{F} < 0$ in this vicinity, which implies that schemes such as MNS_1 are ill-posed for integrating equations (7.7)–(7.8) starting from $\xi_1 = 1$. Integration in the sense of scheme MNS_0, however, remains possible. Again, a breakdown in the numerical solution takes place in a singular fashion, as illustrated in figure 18 where distributions for $w_{\eta_1}(\xi_1, \eta_1 = 0)/c$ and $u_{\eta_1}(\xi_1, \eta_1 = 0)/c$ are shown. We have found from our numerical computations that $\mathscr{F}_{\eta_1}(\xi_1, 0) \propto (\xi_s - \xi_1)^{1/2}$ immediately ahead of ξ_s, which tells us that the breakdown is engendered once again by a Goldstein type singularity. For completeness, profiles for $w_{\eta_1}(\xi_1, \eta_1 = 0)/c$ and $u_{\eta_1}(\xi_1, \eta_1 = 0)/c$ are also presented in figure 19 for the near limit 359.9° 'corner' configuration. These results highlight further the evolution of the singularity with varying β. Observe how results for the case $\beta_0 = s - 1$ (with $s = 359.9/360$) effectively reproduce those of the limit $s \to 1$. Observe also that both components of the wall shear stress tend now to infinitely large values as $\xi_1 \to 0$.

To illustrate the crossflow evolution in region (iii), a selection of profiles for $u(\xi_1, \eta_1)$ is shown in figure 20 for $s = 359.9/360$ and $s \to 1$. Here, we see that the crossflow evolves from a Blasius-like profile at $\xi_1 = 0$ to a massively reversed flow profile at $\xi_1 = 1$. Obviously, this behaviour is tantamount to the formation of a closed streamwise vortex in both cases, and is coupled to a rapid growth in the boundary-layer thickness within the intermediate layer. Note also the excellent agreement between the asymptotic solution for the case $s \to 1$, computed according to (7.11), and the numerical solution for $\xi_1 \lesssim 0.3675$ (see also figure 20 in this regard).

The overall picture emerging from results presented so far, clearly suggests that the flow past a quarter-infinite flat plate is but a regular limit of flows along convex corners, and qualitatively exhibits, on the whole, similar flow characteristics related to the crossflow–vortex structure and eigensolutions emanating from $x = 0$. In this context, it can be said that comments regarding corner flow instability are generally valid for concave and convex corners alike, including the quarter-infinite flat-plate limit.

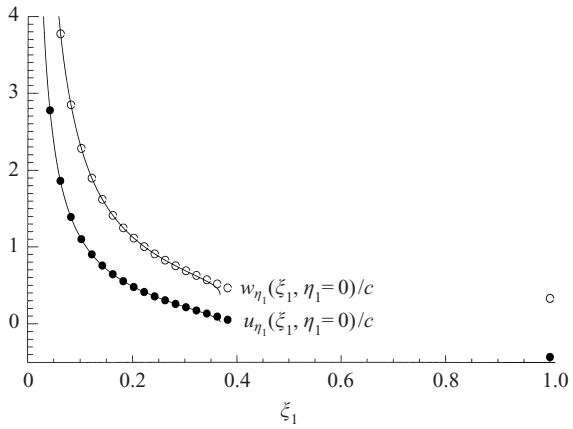

FIGURE 18. Quarter-infinite flat-plate limit numerical (solid lines) and expansions (7.11) (symbols) solutions: variations of $w_{\eta_1}(\xi_1, \eta_1 = 0)/c$ and $u_{\eta_1}(\xi_1, \eta_1 = 0)/c$ with ξ_1.

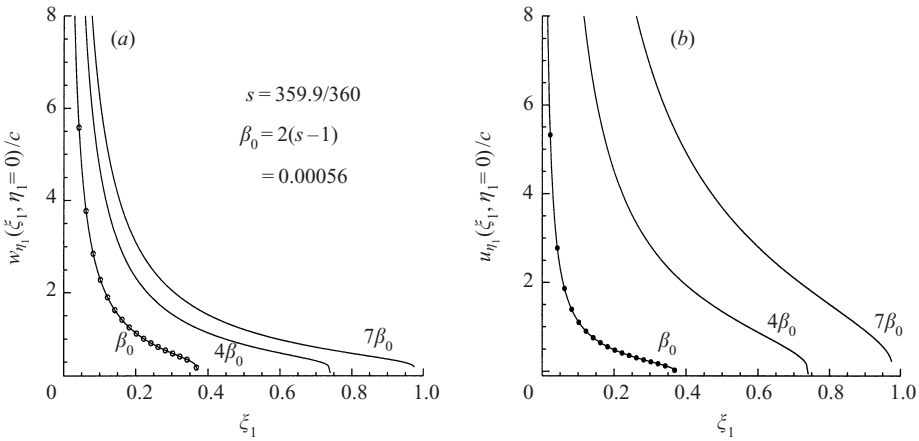

FIGURE 19. Results for 359.9°-convex corner (solid lines) and quarter-infinite flat plate limit (symbols), region (iii): (*a*) $w_{\eta_1}(\xi_1, \eta_1 = 0)/c$ and $u_{\eta_1}(\xi_1, \eta_1 = 0)/c$ distributions, β as indicated.

9. Conclusions and further discussions

In this paper, we have investigated both inviscid and viscous incompressible steady laminar flows along streamwise corners. The formulation is new, quite general, and is applicable to concave and convex corners of arbitrary angles ($\pi - 2\alpha$), including the semi- and quarter-infinite flat-plate limits. Our analysis has unfolded into an inviscid flow problem of the singular perturbation type, leading to an essentially four-region treatment (see figure 2) for the potential flow instead of the one-region traditional approach used by Rubin (1966) for the zero streamwise pressure gradient case (and followed later by other authors: Desai & Mangler 1974; Barclay & Ridha 1980; Wilkinnson & Zamir 1984; Ridha 1990; Dhanak & Duck 1997; amongst others), or the two-region treatment (Smith 1975) employed for the three-dimensional stagnation point flow into a corner. This has necessarily led to a viscous motion characterized by a five-region-structure (depicted in figure 3), compared with the three-region representation hitherto used in previous works: the corner layer (region (i)) is now separated from the far-field boundary layers (regions (ii)) by an interme-

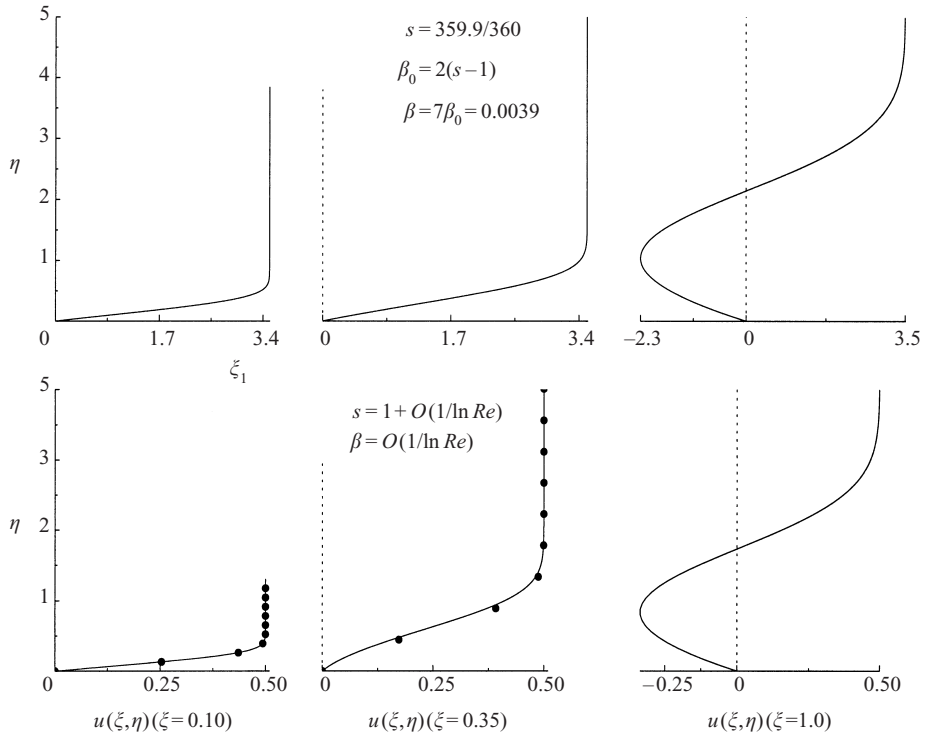

FIGURE 20. 359.9°-convex corner and quarter-infinite flat plate limit $s \to 1$, region (iii): $u(\xi, \eta)$ profiles, β and ξ as indicated; ●, series expansions (7.11) solutions.

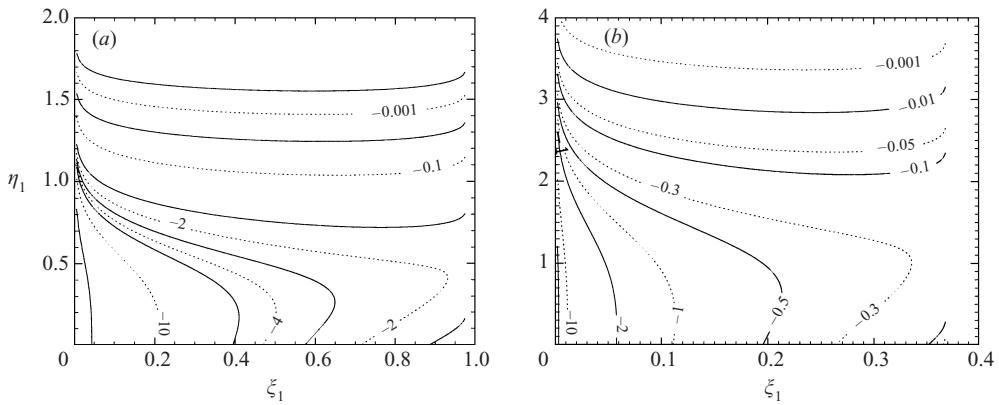

FIGURE 21. Region (iii): constant streamwise vorticity $\omega(\xi_1, \eta_1)$ contours for (*a*) 359.9°-convex corner, $s = 359.9/360$, with $\beta = 7 \times 2(s-1) = 0.0039$, and (*b*) quarter-infinite flat plate limit, $s = 1 + O(1/\ln Re)$.

diate layer (region (iii)), on each of its sides, characterized by spanwise length and velocity scales of $O(\delta)$, where $Re^{-1/2} \ll \delta \ll 1$, with possibly $\delta \sim O(Re^{-1/2} \ln Re)$, as suggested by comparison with the work of Stewartson (1961) on boundary-layer flow past a quarter-infinite flat plate. A major consequence of this structure is a corner-layer motion in convex corners mainly determined by the secondary flow in the (x^*, y^*)-plane, and effectively equivalent to the two-dimensional viscous motion past a wedge, but with similarity solutions being unique and existing only for a favourable

streamwise pressure gradient. Our analysis has further shown that the evolution from this secondary-flow-dominated corner-layer motion into a primary-flow-dominated boundary layer takes place within an extremely short spanwise distance Δx, characterized by $O(Re^{-0.5+\alpha/\pi}\delta^{2\alpha/\pi}) < \Delta x < O(\delta)$, with $-\frac{1}{2}\pi \leqslant \alpha < 0$. For this flow state, the shear stress tends to infinitely large values on approaching the corner-line, leading to infinite streamwise and sideways (particularly as $s \to 1$) forces in the strip $0 < x < \delta,\ z > 0$.

Perhaps the most important result of the present work is that lying in the unravelling of crossflow–vortex structures, previously predicted by Moore (1956) (specifically in the corner layer, but found herein in the intermediate layers), proceeding from the forward corner, for both concave and convex corner flows, including the semi- and quarter-infinite flat plate limiting flow states. These structures give a crucial insight into the nature of corner flows and raise further questions, most worthy of investigating, on their instability, for streamwise vortices in a boundary layer are well known to influence strongly the behaviour of other disturbances (Reed & Saric 1989).

For almost planar corners, the similarity solution for the corner-layer has been found to be non-unique and exhibiting a crossflow with a jetlike or reversed flow profile, depending on the flow state. Similarity equations for the intermediate layer (for the general corner flow problem), on the other hand, possess spanwise algebraically growing eigensolutions, possibly emanating from the corner line; these are believed to be at the origin of many computational difficulties in the numerical task, particularly in obtaining lower branch solutions for concave corners, a problem that we have left unsolved. These difficulties have, for a convex corner, been further compounded by the presence of a Goldstein (1948) type singularity which was partially overcome by using two parabolic implicit marching, second-order finite-difference schemes initiated upstream and downstream of the singularity point.

Crucially, it is only when the said eigensolutions are considered from the viewpoint of independent-Reynolds-number algebraically growing instability (Luchini 1996), that their significance can, perhaps, be best appreciated. In particular, there exist interesting parallels between the spanwise-eigenmodes found by Luchini (1996, 2000), and Anderson, Berggren & Henningson (1999), or between the streamwise-eigenmodes found by Duck *et al.* (1999, 2000) and Duck & Dry (2001), which both algebraically grow in the streamwise direction, and ours. In our results, the eigensolutions are effectively in the spanwise direction; they start becoming dangerous (in the intermediate layer) under sufficiently small pressure gradients conditions (for both solution branches), and grow unboundedly (for the lower solution branch) as $x \to 0$, that is in the inner limit of the intermediate layer which is precisely the outer limit of the corner-layer. Such perturbations naturally lead us to the link between 'bypass transition' and disturbances in algebraic growth suggested by Luchini (1996), which, together with flow instability related to crossflow–vortex structures (Reed & Saric 1989), does seem to be consistent with difficulties reported by Zamir (1981) (see also Zamir & Young 1970, 1979; Barclay 1973) in obtaining a stable corner-layer in laminar form for zero streamwise pressure gradient conditions at a large Reynolds number.

This paper offers, therefore, further explanations (besides those advanced by Ridha 1992; Dhanak & Duck 1997; Duck *et al.* 1999; Parker & Balachandar 1999) for the experimental difficulties, and strongly suggests investigating corner flow instability in the intermediate layer proper, region (iii).

REFERENCES

Anderson, P., Berggren, M. & Henningson, D. S. 1999 Optimal disturbances and bypass transition in boundary layers. *Phys. Fluids* **11**, 134–150.

Barclay, W. H. 1973 Experimental investigation of the laminar flow along a straight 135° corner. *Aero. Q.* **24**, 147–154.

Barclay, W. H. & Ridha, A. H. 1980 Flow in streamwise corners of arbitrary angle. *AIAA J.* **18**, 1413–1420.

Carrier, G. F. 1947 The boundary layer in a corner. *Q. Appl. Maths* **4**, 367–370.

Davis, R. T., Ghia, U. & Ghia, K. N. 1974 Symmetric laminar incompressible flow past sharp wedges. *Comput. Fluids* **2**, 225–235.

Davis, S. F. 1984 A simplified TVD finite difference scheme via artificial viscosity. *ICASE Rep.* 84–53.

Desai, S. S. & Mangler, K. W. 1974 Incompressible laminar boundary layer flow along a corner formed by two intersecting planes. *RAE Tech. Rep.* 74062.

Dhanak, M. R. & Duck, P. W. 1997 The effects of freestream pressure gradient on corner boundary layer. *Proc. R. Soc. Lond.* A **453**, 1793–1815.

Duck, P. W. & Dry, S. L. 2001 On a class of unsteady, non-parallel, three-dimensional disturbances to boundary-layer flows. *J. Fluid Mech.* **441**, 31–65.

Duck, P. W., Stow, S. R. & Dhanak, M. R. 1999 Non-similarity solutions to the corner boundary-layer equations (and the effects of wall transpiration). *J. Fluid Mech.* **400**, 125–162.

Duck, P. W., Stow, S. R. & Dhanak, M. R. 2000 Boundary-layer flow along a ridge: alternatives to the Falkner–Skan solutions. *Phil. Trans. R. Soc. Lond.* A **358**, 3075–3090.

El-Gamal, H. 1977 Laminar flow along a corner with boundary layer suction. PhD thesis, University of London.

Ghia, K. N. 1975 Incompressible streamwise flow along an unbounded corner. *AIAA J.* **7**, 902–907.

Goldstein, S. 1948 On laminar boundary-layer flow near a point of separation. *Q. J. Mech. Appl. Maths* **1**, 43–69.

Gurevich, Yu. G. 1981 Boundary layer in the neighbourhood of the intersection of a cylindrical surface and a plane. *Mekh. Zhid. i Gaza* **2**, 160–165 (Engl. transl. *Fluid Dyn.* **16**(2), 285–289).

Gurevich, Yu. G. 1985 Viscous fluid flow near the line of intersection of curved surfaces. *Mekh. Zhid. i Gaza* **3**, 16–21 (Engl. transl. *Fluid Dyn.* **20**(3), 348–352).

Libby, P. A. & Fox, H. 1963 Some perturbation solutions in laminar boundary-layer theory. *J. Fluid Mech.* **17**, 433–449.

Loitsianskii, L. G. 1936 Interference of boundary layers. *Central Aero-Hydrodyn. Inst. Rep.* 249, Moscow (Engl. transl. ARC 3186-FM342).

Loitsianskii, L. G. & Bolshakov, V. P. 1936 The boundary layer in a corner. *Central Aero-Hydrodyn. Inst. Rep.* 279, Moscow (Engl. transl. NACA-TM-1308).

Luchini, P. 1996 Reynolds-number-independent instability of the boundary layer over a flat surface. *J. Fluid Mech.* **327**, 101–115.

Luchini, P. 2000 Reynolds-number-independent instability of the boundary layer over a flat surface: optimal perturbations. *J. Fluid Mech.* **404**, 289–309.

Moffat, H. K. 1964 Viscous and resistive eddies near a sharp corner. *J. Fluid Mech.* **18**, 1–18.

Moore, F. K. 1956 Three-dimensional boundary layer theory. *Adv. Appl. Mech.* **4**, 159–228.

Neiland, V. Ya. 1969 Theory of laminar boundary-layer separation in supersonic flow. *Mekh. Zhid. i Gaza* **4**, 53–57 (Engl. transl. *Fluid Dyn.* **4**(4), 33–35).

Pal, A. & Rubin, S. G. 1971 Asymptotic features of viscous flow along a corner. *Q. Appl. Maths* **29**, 91–108.

Parker, S. J. & Balachandar, S. 1999 Viscous and inviscid instabilities of flow along a streamwise corner. *Theoret. Comput. Dyn.* **31**, 231–270.

Pearson, J. R. A. 1957 Homogeneous turbulent and laminar viscous flow. PhD thesis, Cambridge University.

Reed, H. L. & Saric, W. S. 1989 Stability of three-dimensional boundary layers. *Annu. Rev. Fluid Mech.* **21**, 235–284.

Ridha, A. H. 1978 Laminar flow along corners having arbitrarily large transverse curvature. PhD thesis, University of London.

Ridha, A. 1990 Sur la couche limite incompressible laminaire le long d'un dièdre. *C. R. Acad. Sci. Paris* **311**, sér. II, 1123–1128.

Ridha, A. 1992 On the dual solutions associated with boundary-layer equations in a corner. *J. Engng Maths* **26**, 525–537.

Ridha, A. 1995 L'écoulement potentiel tridimensionnel le long d'un coin revisité. *C. R. Acad. Sci. Paris* **321**, sér. II*b*, 481–487.

Ridha, A. 1996 Three-dimensional mixed convection laminar boundary-layer near a plane of symmetry. *Intl J. Engng Sci.* **34**(6), 659–675.

Rosenhead, L. 1966 *Laminar Boundary Layers*. Oxford University Press.

Rubin, S. G. 1966 Incompressible flow along a corner. *J. Fluid Mech.* **26**, 169–186.

Rubin, S. G. & Grossman, B. 1971 Viscous flow along a corner. Part 2. Numerical solution of corner-layer equations. *Q. Appl. Maths* **29**, 169–186.

Smith, F. T. 1975 Three-dimensional stagnation point flow into a corner. *Proc. R. Soc. Lond.* A **334**, 489–507.

Stewartson, K. 1961 Viscous flow past a quarter-infinite plate. *J. Aero. Sci.* **28**, 1–10.

Stewartson, K. & Williams, P. G. 1969 Self induced separation. *Proc. R. Soc. Lond.* A **312**, 181–206.

Sun, M. & Takayama, K. 1999 Conservative smoothing on an adaptive quadrilateral grid. *J. Comput. Phys.* **150**, 143–180.

Sychev, V. V., Ruban, A. I., Sychev, V. V. & Korolev, G. L. 1998 *Asymptotic Theory of Separated Flows*. Cambridge University Press.

Van Dyke, M. 1975 *Perturbation Methods in Fluid Mechanics*, Annotated edn, Academic.

Wilkinson, S. R. & Zamir, M. 1984 Cross-flow and vorticity patterns in the corner boundary layer at different corner angles. *Aero. Q.* **35**, 309–316.

Yee, H. C. 1987 Construction of explicit and implicit symmetric TVD schemes and their applications. *J. Comput. Phys.* **68**, 151–179.

Zamir, M. 1981 Similarity and stability of laminar boundary in a streamwise corner. *Proc. R. Soc. Lond.* A **377**, 269–288.

Zamir, M. & Young, A. D. 1970 Experimental investigation of the boundary layer in a streamwise corner. *Aero. Q.* **21**, 313–339.

Zamir, M. & Young A. D. 1979 Pressure gradient and leading edge effects on corner boundary layer. *Aero. Q.* **30**, 471–484.